078 Measurement of Oil Thickness on Water from Aircraft:

A. Active Microwave Spectroscopy

B. Electromagnetic Thermoelastic Emission

The Environmental Studies Research Funds are financed from special levies on the oil and gas industry and administered by the Canada Oil and Gas Lands Administration for the Minister of Energy, Mines and Resources, and by the Northern Affairs Program for the Minister of Indian Affairs and Northern Development.

The Environmental Studies Research Funds and any person acting on their behalf assume no liability arising from the use of the information contained in this document. The opinions expressed are those of the authors and do not necessarily reflect those of the Environmental Studies Research Funds agencies. The use of trade names or identification of specific products does not constitute an endorsement or recommendation for use.

Environmental Studies Research Funds

Report No. 078

August 1987

MEASUREMENT OF OIL THICKNESS ON WATER FROM AIRCRAFT:

A. Active Microwave Spectroscopy;
B. Electromagnetic Thermoelastic Emission

E.M. Reimer
J.R. Rossiter

Canpolar Inc.
421 Eglinton Ave. West
Toronto, Ontario
M5N 1A4

Scientific Adviser: R. Goodman

92-01750/

The correct citation for this report is:

Reimer, E.M., Rossiter, J.R., 1987. Measurement of oil thickness on water from aircraft: A. Active microwave spectroscopy; B. Electromagnetic thermoelastic emission. Environmental Studies Research Funds Report No. 078. Ottawa, viii + 82 p.

Published under the auspices
of the Environmental Studies
Research Funds
ISBN - 0-920783-77-5
©1987 - Canpolar Inc.

Canpolar Project No. 1044

TABLE OF CONTENTS

Page

SUMMARY 1

RÉSUMÉ 4

A. ACTIVE MICROWAVE SPECTROSCOPY

1. INTRODUCTION 7
   1.1 SYSTEM CONCEPT 7

2. THEORY 9
   2.1 BACKGROUND 9
   2.2 DIELECTRIC PROPERTIES OF WATER 9
   2.3 DIELECTRIC PROPERTIES OF OILS 11
   2.4 THREE-LAYER THEORETICAL MODEL 11
   2.5 THEORETICAL RESULTS 18
   2.6 FOOTPRINT SIZE 23
   2.7 ROUGH OCEAN SURFACE 24

3. EXPERIMENTAL MEASUREMENTS 27
   3.1 METHOD 27
      3.1.1 Experimental set-up 27
      3.1.2 Radar and spectrum analyzer calibration . . . 29
      3.1.3 Dielectric constant of sand 31
   3.2 RESULTS 31
   3.3 DISCUSSION 35
      3.3.1 Radar pulse characteristics 35
      3.3.2 Spectral analysis of the radar output 37
      3.3.3 Pulse-length limitations 37
      3.3.4 Summary and conclusions 38

4. DISCUSSION AND RECOMMENDATIONS 39
   4.1 CONCLUSIONS 39
   4.2 RECOMMENDATIONS FOR FURTHER WORK 39

B. ELECTROMAGNETIC THERMOELASTIC EMISSION

1. INTRODUCTION 42
   1.1 BACKGROUND 42
   1.2 OUTLINE OF REPORT 43

2. THEORETICAL FEASIBILITY 45
   2.1 IRRADIATION TECHNIQUES 45
   2.2 THERMOELASTIC RESPONSE 47
      2.2.1 Nd:Yag Laser 50
      2.2.2 CO_2 laser 54
      2.2.3 X-band radar 54

Page

2.3 ACOUSTIC BEHAVIOUR OF OIL FILMS 55
2.3.1 Acoustic characteristics 55
2.3.2 Expected response 59
2.4 DETECTION OF THERMOELASTIC RESPONSE 61
2.4.1 Acoustic methods 61
2.4.2 Optical Interferometry 64
2.5 SUMMARY 65

3. EXPERIMENTAL VERIFICATION 67
3.1 METHOD 67
3.2 RESULTS 69
3.3 CONCLUSIONS 71

4. SYSTEM DESIGN AND RECOMENDATIONS 72
4.1 SYSTEM DESCRIPTION 72
4.1.1 Optical unit 72
4.1.2 Control unit 75
4.1.3 Discussion 75
4.2 RECOMMENDATIONS 77

APPENDIX A PHYSICAL DISPLACEMENT CALCULATION 79

REFERENCES 80

LIST OF TABLES

Table		Page
1.	Typical irradiation sources	46
2.	Symbols and units for acoustic response	49
3.	Physical properties of liquids	51
4.	Attenuation rate (α) vs wavelength for oil and sea-water	51
5.	Thermoelastic conversion efficiency	51
6.	Approximate acoustic power and mechanical displacement for three sources described in Table 1	53
7.	Sound velocity and attenuation in various liquids	56
8.	Oil slick thickness measurement system timing sequence	76

LIST OF FIGURES

Figure		Page
1.	Active microwave spectroscopy concept	8
2.	Dielectric properties of (a) pure water and (b) sea-water with DC conductivity of 5 S/m	10
3.	Dielectric constant of oil	12
4.	Sketch of geometry - three-layer case	13
5.	Calculated reflection coefficient as a function of frequency for different thicknesses of second layer	16
6.	Calculated reflection coefficient for oil over pure water at 20°C as a function of frequency for various thicknesses of oil layer. Dielectric constant of oil is 2.25	20
7.	Calculated reflection coefficient for oil over sea-water at 20°C as a function of frequency for various thicknesses of oil layer. Dielectric constant of oil is 2.25	21
8.	Calculated reflection coefficient for oil over sea-water at 0°C as a function of frequency for various thicknesses of oil layer. Dielectric constant of oil is 2.25	22
9.	Calculated reflection coefficient for oil over sea-water at 20°C as a function of frequency for various thicknesses of oil layer. Dielectric constant of oil is 3	22
10.	Sketch of active microwave spectroscopy over rough ocean	26
11.	Experimental set-up using impulse radar system over sand and water	28
12.	Radar window calibration	30
13.	Dielectric constant of sand	32
14.	Reflection coefficient for 5 cm sand layer over water as a function of frequency	33
15.	Reflection coefficient for 14-cm layer over water as a function of frequency	34
16.	Impulse transmitter output pulse	36

Figure Page

17. Geometry of electromagnetic thermoelastic source irradiating an oil layer on water 52

18. Calculated oil layer thickness vs. acoustic reverberation frequency, for a sound velocity of 1,300 m/s 58

19. Idealized acoustic response from an oil layer about 20 mm thick stimulated by a short, high-power laser pulse . 60

20. Attenuation rates of sound in water as a function of frequency 62

21. Ambient acoustic noise in the ocean as a function of frequency 63

22. Experimental set-up for testing interferometric detection of oil film thermoelastic response 68

23. Experimental test results with two different time scales . 70

24. Operating scenario for oil slick thickness measurement system 73

25. Oil slick thickness measurement system block diagram . . . 74

SUMMARY

This report examines the technical feasibility of using two new techniques for airborne measurement of the thickness of an oil layer on water: active microwave spectroscopy and electromagnetic thermoelastic emission.

Active microwave spectroscopy uses changes in surface reflectivity as a function of radar frequency. Oil provides an excellent dielectric match to water over the frequency range from about 50 to 500 GHz. Hence destructive interference effects will give nulls in surface reflectivity at frequencies related to the thickness of the oil layer.

A theoretical assessment of this technique was made using plane layer theory for complex dielectrics. Nulls in the reflectivity were 5 to 15 dB in amplitude. The rate of beating in received spectra as a function of radar frequency is directly proportional to the oil thickness. Uncertainty in the thickness estimate obtained for an unknown oil will be determined by the dielectric constant of the oil and is estimated to be less than $\pm$15%. Effects of rough oceans were not examined in detail, but do not appear to be severe. A simple experiment using a wide-band pulse with a centre frequency of 400 MHz and a real-time spectrum analyser did not provide satisfying confirmation of the theory. Subsequent analysis showed that the experimental procedure was flawed, and that discrete frequency measurements over a wide frequency band should be used.

These results suggest that an airborne active microwave

system measuring surface reflectivity over 50 to 400 GHz at frequency intervals of a few GHz, could be used to estimate oil thicknesses from 0.1 to 30 mm. The lower bound of thickness will be determined by the highest radar frequency used. The upper bound will be determined by the sampling interval in the frequency domain; thicker oil layers could give ambiguous results because of aliasing.

In the electromagnetic thermoelastic emission technique, the oil is illuminated with electromagnetic energy, some of which is converted to acoustic energy because of local heating effects. The acoustic response is indicative of the thickness of the oil.

An order-of-magnitude theoretical assessment of this technique was made. Lasers and radar transmitters appear to be capable of generating sufficiently strong excitation at a range of about 20 meters. Microphone detection does not appear to be practical; hydrophone detection, although possible, is not ideal. However, detection of the mechanical displacement using optical interferometry appears suitable. A simple laboratory verification was made through the courtesy of the Industrial Materials Research Institute in Montreal which has succeeded in developing optical interferometry as a industrial tool. The thickness of about 1 cm of Hibernia crude oil in a beaker was measured at a range of about 1 m. The results appeared to be relatively insensitive to motion of the sample.

These results suggest that electromagnetic thermoelastic emission would be able to measure the thickness of oil from 0.1 to

10 mm. The major inaccuracy in the measurement is expected to be uncertainty in the velocity of acoustic waves in the oil, estimated to be ±20%. Components for a prototype system are commercially available except for the interferometer, and a preliminary system design is described here.

For both techniques full-scale experimental verification in a wave basin is recommended in order to determine the feasibility and cost of prototype systems. The required equipment is readily available and there are several appropriate test facilities in Canada.

RÉSUMÉ

Ce rapport examine la faisabilité technique de l'utilisation de deux nouvelles techniques pour la mesure aéroportée de l'épaisseur d'une couche de pétrole sur l'eau: la spectoscopie à micro-ondes actives et l'émission thermoélastique électromagnétique.

La spectoscopie à micro-ondes actives utilise les changements de réflexivité de la surface comme fonction de la fréquence radar. Le pétrole constitue un correspondant diélectrique excellent pour l'eau sur les ondes de fréquence d'environ 50 à 500 GHz. Ainsi les effets d'interférence destructifs donneront des résultats nuls dans la réflexivité de la surface à des fréquences liées à l'épaisseur de la couche de pétrole.

Une évaluation théorique de la technique a été réalisée avec l'utilisation de la théorie de la couche de plans pour le diélectrique complexe. Les zéros de réflexivité avaient une amplitude de 5 à 15 dB. Le taux de battement en spectra reçus en tant que fonction de la fréquence radar est directement proportionnel à l'épaisseur du pétrole. L'incertitude dans l'estimation d'épaisseur obtenue pour un pétrole inconnu, sera déterminée par la constante diélectrique du pétrole et elle est estimée à moins de $\pm$15%. Les effets de l'agitation de l'océan n'ont pas été étudiés en détail, mais ne semblent pas être considérables. Une simple expérience utilisant une impulsion à larges bandes avec une fréquence centrale de 400 MHz et un analyseur de spectre à temps réel n'a pas confirmé la théorie de façon satisfaisante.

Les analyses suivantes ont montré que des erreurs ont été faites pendant l'expérience, et que des mesures de fréquence discrètes sur une bande de fréquence large devraient être utilisés.

Sur la base de ces résultats, il semble qu'un système aéroporté de micro-ondes qui mesure la réflexivité de la surface sur 50 à 400 GHz à intervalles de fréquence de quelques GHz pourrait être utilisé pour faire une estimation de l'épaisseur du pétrole de 0,1 à 30mm. La limite inférieure est déterminée par la plus haute fréquence radar utilisée. La limite supérieure est déterminée par l'intervalle de l'échantillon dans le domaine de la fréquence; des couches de pétrole plus épaisses pourraient donner des résultats ambigus en raison de «l'aliasing».

Dans la technique de l'émission thermoélastique électromagnétique, le pétrole est illuminé à l'aide de l'énergie electromagnétique et une partie de celle-ci est transformée en énergie acoustique en raison des effets de la chaleur locale. La réponse acoustique indique l'épaisseur de la couche de pétrole.

Une évaluation théorique d'ordre de grandeur de cette technique a été réalisée. Les transmetteurs radar et laser semblent capables de générer une excitation suffisamment forte à une portée d'environ 20 mètres. La détection par microphone ne semble pas pratique; la détection hydrophone, bien que possible, n'est pas la solution idéale. Cependant, la détection du déplacement mécanique par interférométrie optique semble convenir. Une simple vérification de laboratoire a été faite grâce à la courtoisie de l'Institut de génie des matériaux (IGM)

(Industrial Materials Research Institute) à Montréal. Ce groupe a réussi à mettre au point l'interférométrie optique comme outil industriel. L'épaisseur d'environ 1 cm de pétrole brut d'Hibernia dans un bécher a été mesurée à une portée d'environ 1m. Les résultats semblaient être relativement insensibles au mouvement de l'échantillon.

Ces résultats suggèrent que l'émission électromagnétique thermoélastique pourrait mesurer l'épaisseur du pétrole de 0,1 à 10mm. La principale incertitude sera probablement le peu de connaissance de la vélocité des ondes acoustiques dans le pétrole, estimée à $\pm$20%. Les éléments d'un système prototype sont disponibles sur le marché, sauf pour ce qui est de l'interféromètre, et la description d'un projet de système préliminaire est jointe.

Une vérification expérimentale complète des deux techniques dans un bassin à vagues est conseillée afin de déterminer la faisabilité et le coût des prototypes. L'équipement nécessaire est facile à obtenir et il existe plusieurs endroits disposant des installations appropriées au Canada.

A. ACTIVE MICROWAVE SPECTROSCOPY

1. INTRODUCTION

1.1 SYSTEM CONCEPT

Detection of oil slicks on the ocean has been well verified by passive microwave techniques at frequencies from 5 to 90 GHz (Sorensen 1984), indicating that the oil is disturbing the ocean surface emissivity at these frequencies. However, these techniques are usually made at a single frequency and do not give independent estimates of slick thickness. In this report, the porsibility of using active microwave spectroscopy to estimate slick thickness is examined.

The system concept is illustrated in Figure 1. An oil layer on the water surface will selectively absorb incident radiation when the layer is one-quarter wavelength thick, or certain integral multiples thereof, due to interference within the layer. This fact implies that the backscattered signal will show nulls at the frequencies corresponding to these wavelengths. By measuring the backscattered radiation over a wide enough bandwidth, oil layer thickness can be determined, averaged over the area of the illuminated footprint.

1.2 OUTLINE OF REPORT

Discussion of the physics and development of a theoretical model are given in Chapter 2; a description of some very simple experimental results using impulse radar are presented in Chapter 3; and a summary of further experimental effort required is found in Chapter 4.

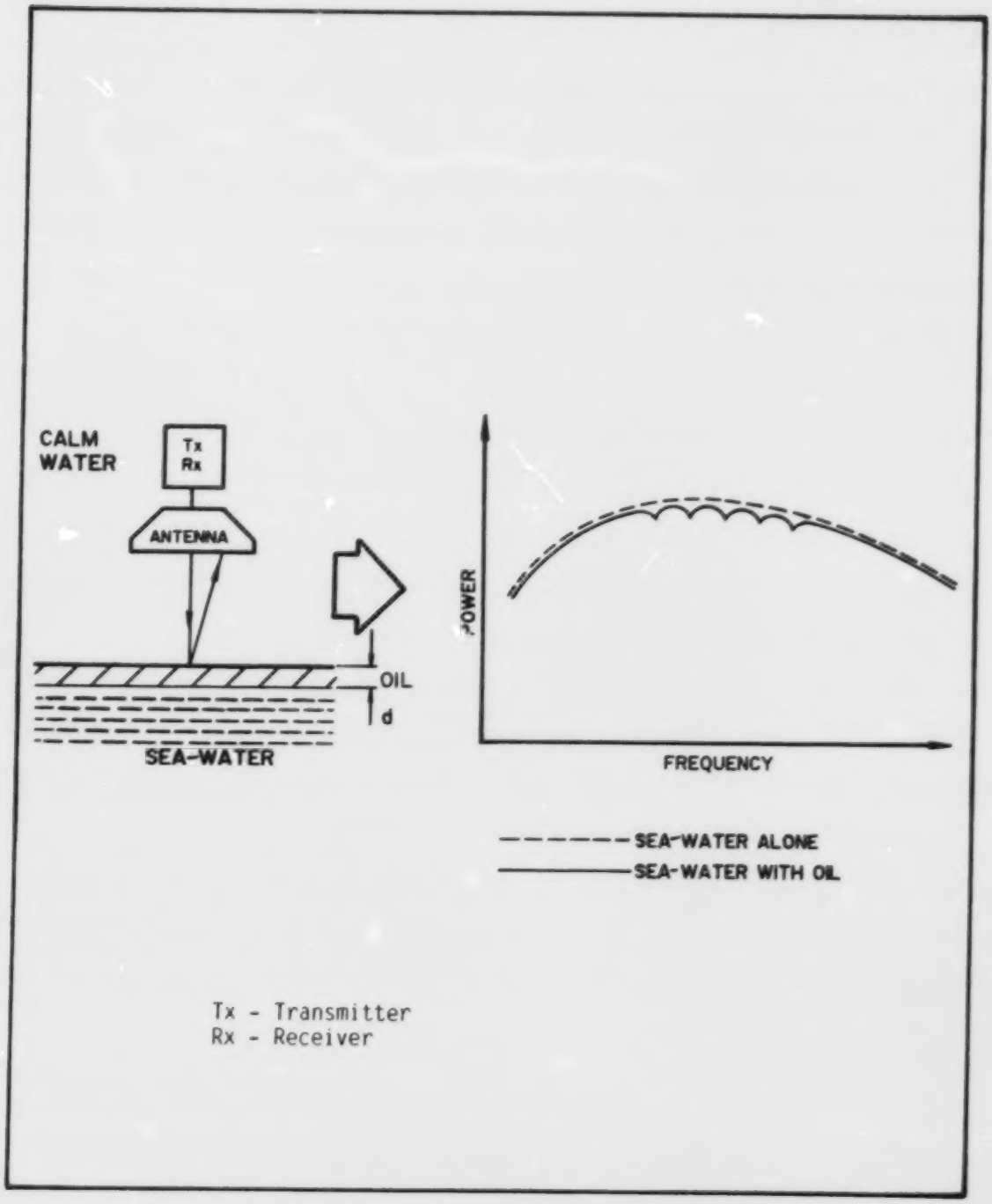

Figure 1 Active microwave spectroscopy concept

2. THEORY

2.1 BACKGROUND

Oil slick thickness detection using the spectroscopic approach will depend on:

- backscatter intensity from the air-oil and oil-water interfaces;
- thin film coupling effects; and
- effects of surface roughness and non-uniform film thicknesses.

The physics of these phenomena is well known for plane layers. Backscatter intensity inclusive of thin film coupling can be calculated from the known complex dielectric constants for oil and water.

2.2 DIELECTRIC PROPERTIES OF WATER

The dielectric properties of water are dominated in the microwave frequency range by the temperature-dependent Debye relaxation of the polar water molecule near 10 GHz. The real part of the dielectric constant drops from about 80 to about 5, and the dielectric absorption shows a peak at the relaxation frequency. In addition, sea-water has a DC conductivity of about 5 S/m, giving additional losses with a magnitude that is inversely proportional to frequency (von Hippel 1954; Vant 1976).

The real (ϵ') and imaginary (ϵ'') parts of the complex dielectric constant for pure water, calculated after Royer (1973) are shown in Figure 2(a) for $0^{o}C$ and $20^{o}C$. Similar plots showing the effect of 5 S/m DC conductivity of sea-water are shown in Figure 2(b).

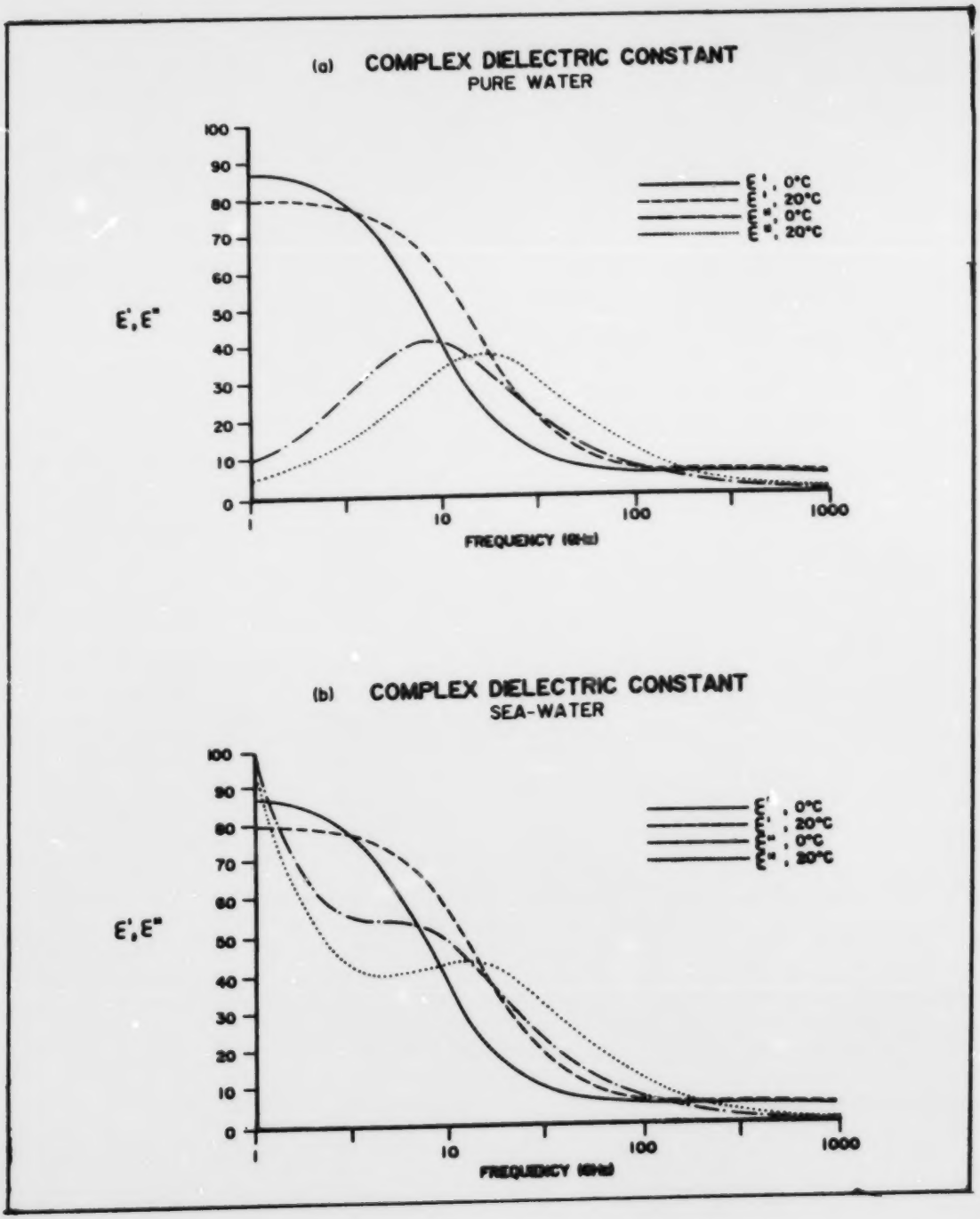

Figure 2 Dielectric properties of (a) pure water and (b) sea-water with DC conductivity of 5 S/m

2.3 DIELECTRIC PROPERTIES OF OILS

The dielectric properties of oils over this frequency range appear much more straightforward, exhibiting neither great frequency nor temperature dependence. The loss terms are very small. There may be some modification to the properties due to mixing with water, but this effect is also expected to be relatively small.

The published values of dielectric properties for various crude and refined oils are summarized in Figure 3. Measurements made at frequencies of 37 GHz and 68 GHz, for example, show the dielectric constant ranging from 1.85 to 2.94. An API 20 Gravity crude oil at 23°C has a dielectric constant of 2.29 (C-CORE 1978). More recent measurements by MacDougall and Tunaley (1986) for crude oil confirm these values, as shown in Figure 3.

2.4 THREE-LAYER THEORETICAL MODEL

The simplest situation to consider is a three-layer dielectric sandwich, shown in Figure 4. The reflection at each interface at normal incidence will be given by (Brekhovskikh 1960):

$$V_{21} = \frac{\sqrt{\varepsilon_1} - \sqrt{\varepsilon_2}}{\sqrt{\varepsilon_1} + \sqrt{\varepsilon_2}} \qquad [2.1]$$

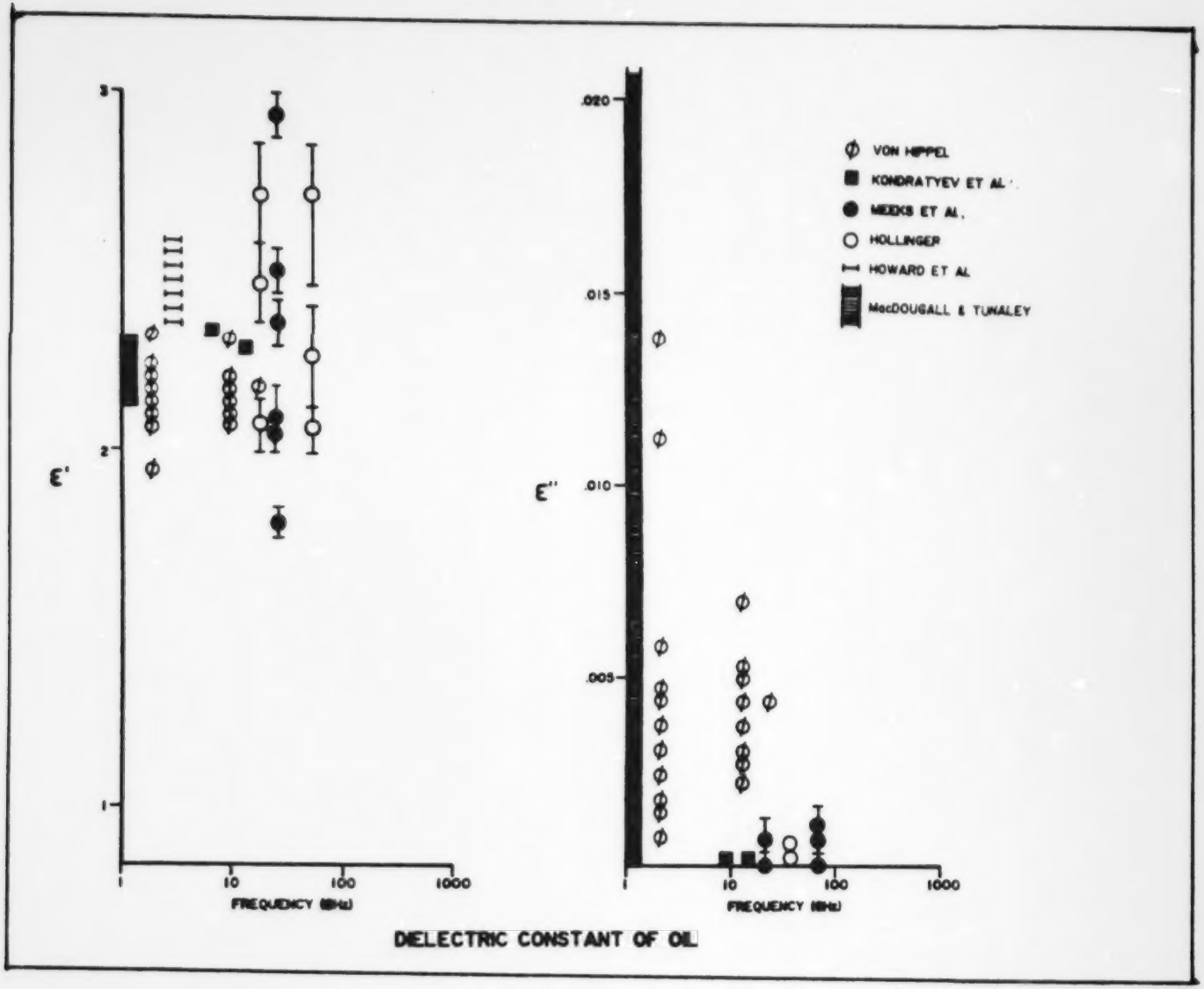

Figure 3 Dielectric constant of oil (modified from C-CORE 1978)

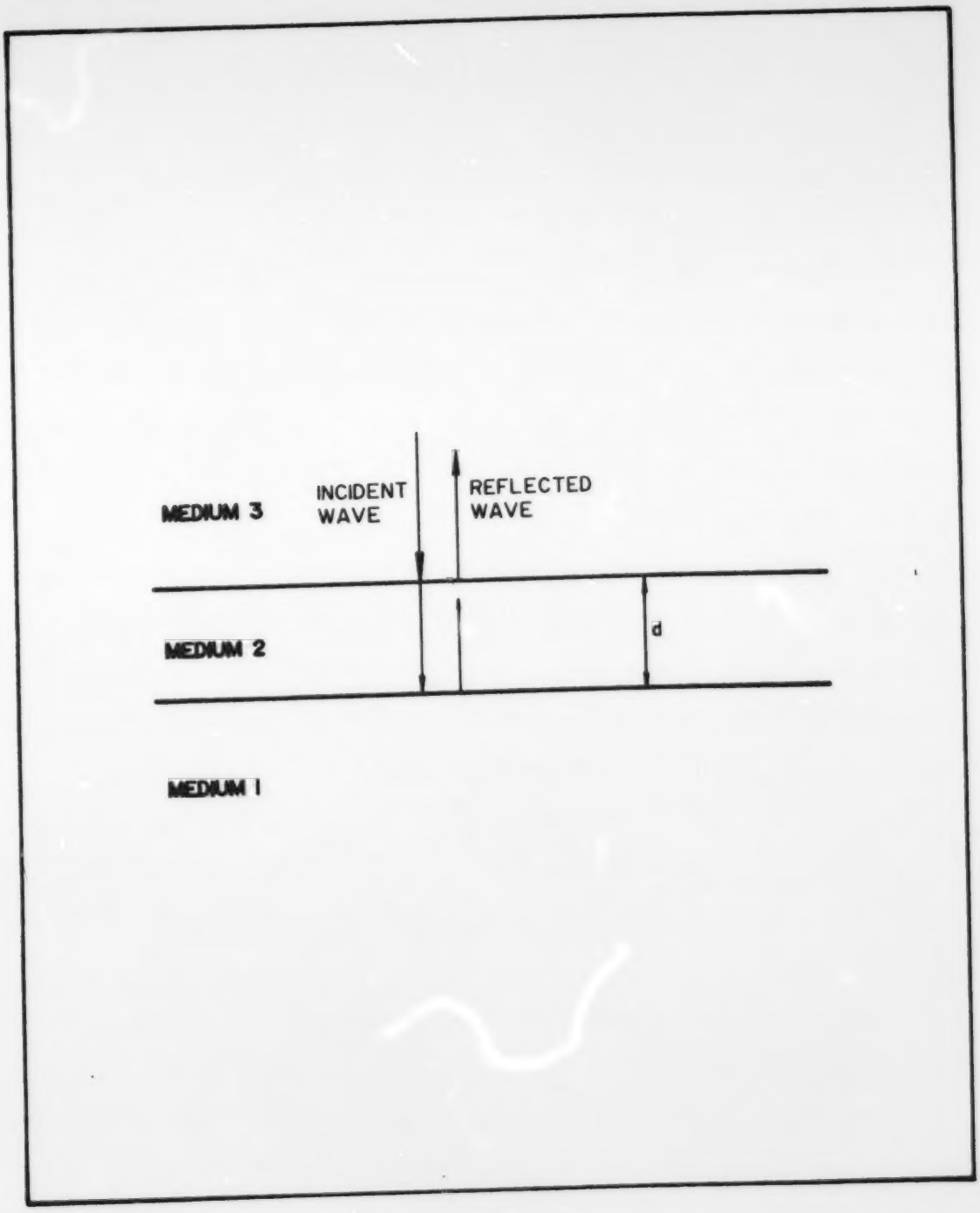

Figure 4 Sketch of geometry - three-layer case

where

V_{21} = reflection coefficient at first (2-1) interface at normal incidence;

$\varepsilon_1, \varepsilon_2$ = complex dielectric constants of layer 1 and 2 respectively.

When a second interface is added, there will be interference set up between the waves reflected from the 3-2 interface and the 2-1 interface. Therefore, the effect of thickness becomes important, because if the layer is a quarter-wavelength thick (or multiples 3/4, 5/4, etc.), the interference will be destructive, and the resulting reflection will be minimized. This phenomenon is the principle behind conventional optical non-reflective coatings (e.g., Sears 1949), and gives the coloured bands seen visually on thin oil slicks.

Optimum matching occurs when the dielectric properties of the three layers are related by:

$$n_2 = \sqrt{n_1 n_3} \qquad [2.2]$$

where n_j = complex index of refraction of the jth layer

$= \sqrt{\varepsilon_j}$

ε_j = complex dielectric constant of the jth layer.

Note that n_j and ε_j are frequency-dependent in general.

The full expression for the complex reflection coefficient of a three-layer model at normal incidence is given by:

$$V = \frac{n_2 (n_3 - n_1) \cos\alpha d - i (n_1 n_3 - n_2^2) \sin\alpha d}{n_2 (n_3 + n_1) \cos\alpha d - i (n_1 n_3 + n_2^2) \sin\alpha d} \qquad [2.3]$$

where:

V = complex reflection coefficient,

d = thickness of layer 2,

$\alpha = 2\pi / \lambda_2$,

λ_2 = wavelength in layer 2 = $\dfrac{3 \times 10^8}{f\, n_2}$

f = frequency (Hz),

$i = \sqrt{-1}$.

The power reflection coefficient is $|V|^2$.

For $n_3 = 1$ and n_2 real (non-lossy), and $n_1 = x + iy$, equation 2.3 reduces to:

$$V = \frac{n_2 (1-x) \cos\alpha d + y \sin\alpha d - i [\, n_2 y \cos\alpha d + (x - n_2^2) \sin\alpha d]}{n_2 (1+x) \cos\alpha d + y \sin\alpha d - i [-n_2 y \cos\alpha d + (x + n_2^2) \sin\alpha d]} \qquad [2.4]$$

Examples of V for $\varepsilon_1 = 6$ and $\varepsilon_2 = 2.25$ (no loss), are shown in Figure 5.

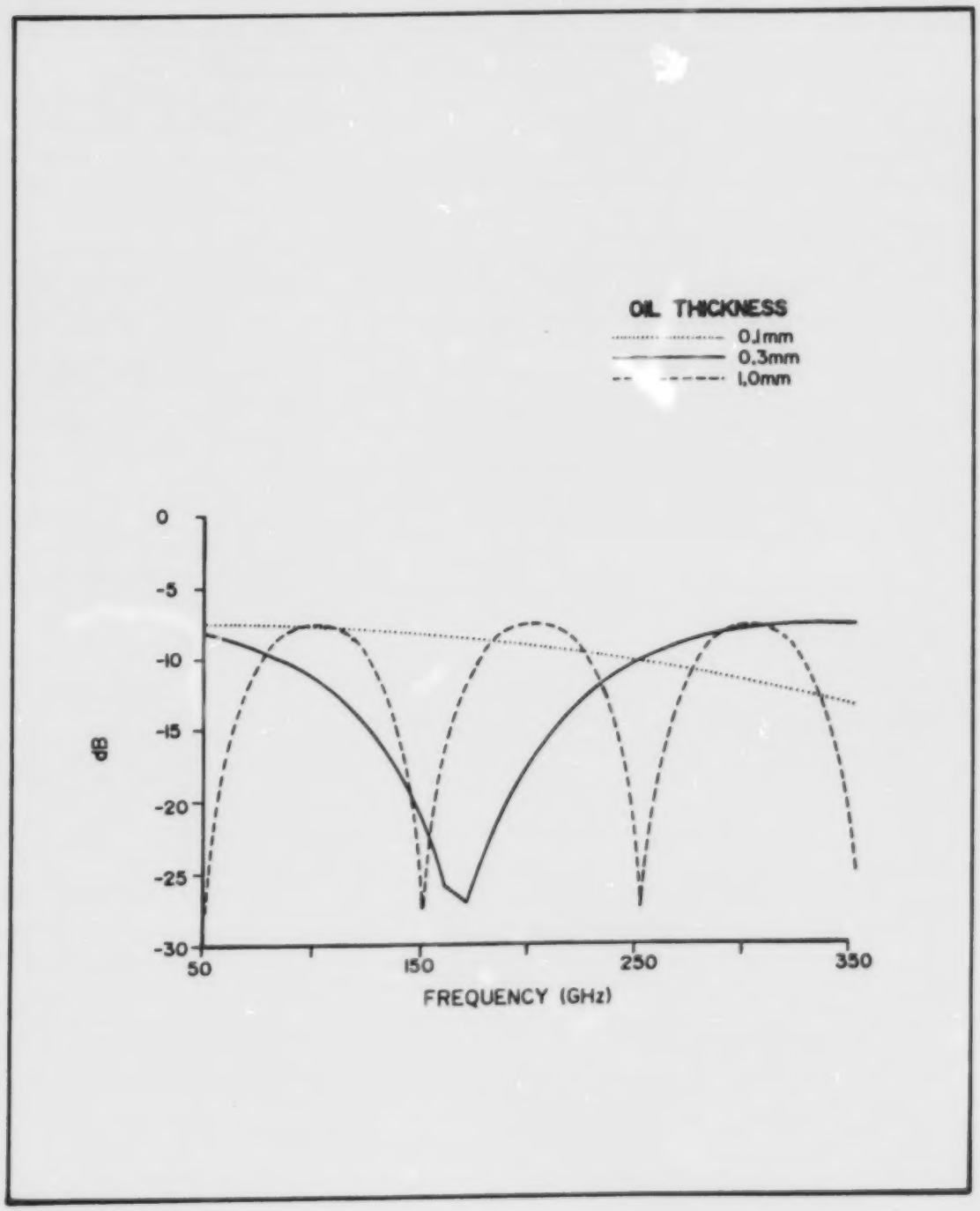

Figure 5 Calculated reflection coefficient as a function of frequency for different thicknesses of second layer

As the thickness of the middle layer increases, the frequency at which the first null is observed decreases. Moreover, the rate of beating of the interference (as a function of radio frequency) is proportional to the thickness of the middle layer. This beating rate can be derived from equation 2.3 or 2.4, which have terms in the form:

$$\cos(\alpha d) = \cos\left[\frac{2\pi n_2 f}{3 \times 10^8} d\right] \qquad [2.5]$$

where f is in Hz and d is in meters.

Therefore, V will exhibit minima when αd changes by π radians, i.e. when the frequency change, Δf is:

$$\Delta f = \frac{3 \times 10^8}{2 n_2 d} \text{ Hz.} \qquad [2.6]$$

For example, for $n_2 = 1.5$ and $d = 1$ mm, $\Delta f = 100$ GHz, as seen in Figure 5.

Hence, from equation 2.6,

$$d = \frac{1.5 \times 10^8}{\sqrt{\epsilon_2}\ \Delta f} \text{ m.} \qquad [2.7]$$

Because ϵ_2 varies only slightly for various oils and enters equation 2.7 as a square root, equation 2.7 can be used to determine oil layer thickness with a maximum uncertainty for an unknown oil of $\pm$15%.

2.5 THEORETICAL RESULTS

Sets of calculated reflection coefficients, for the frequency range from 50 to 350 GHz, are shown in Figures 6 to 9 for various thicknesses of oil, based on equation 2.4. The dielectric constant of the oil is 2.25 (except in Figure 9) and real. The dielectric constant of the water is as shown in Figure 2 -- i.e., complex and frequency-dependent.

Reflection coefficient values for oil over pure water are shown in Figure 6. For oil layers thinner than about 0.1 mm nulls are above the frequency range shown. As the oil layer becomes thicker, the first null moves down in frequency, and a 1-mm thick layer has several nulls in the frequency range. As the oil becomes thicker, the spacing of the nulls is closer. For an oil layer 3 mm thick, the spacing is about 30 GHz.

Values for oil over sea-water (Figure 7) show almost no difference to those for oil over pure water, indicating that the reflection coefficient is not greatly influenced by the losses in the underlying water at these frequencies.

The values for oil over sea-water at a temperature of $0^{o}C$ are shown in Figure 8. They are very similar to those shown in Figure 7, but a few dB lower because of the slightly greater value of the dielectric constant of water at $0^{o}C$ (in this frequency range). The positions of the nulls do not change. An oil of slightly higher dielectric constant, 3.0, was also examined as shown in Figure 9. The greater dielectric constant alters the position of the nulls because of the change in wavelength in the

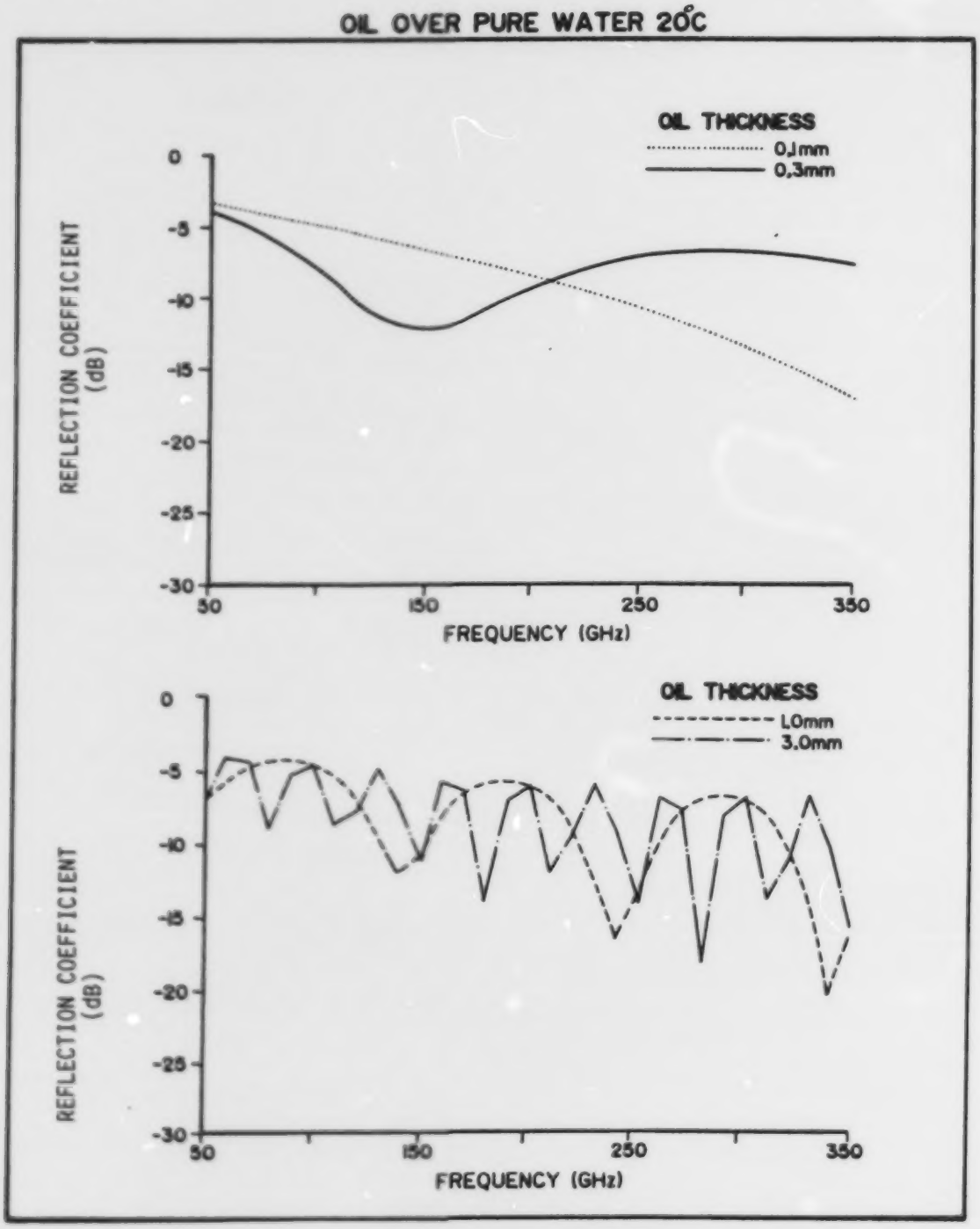

Figure 6 Calculated reflection coefficient for oil over pure water at 20°C as a function of frequency for various thicknesses of oil layer. Dielectric constant of oil is 2.25.

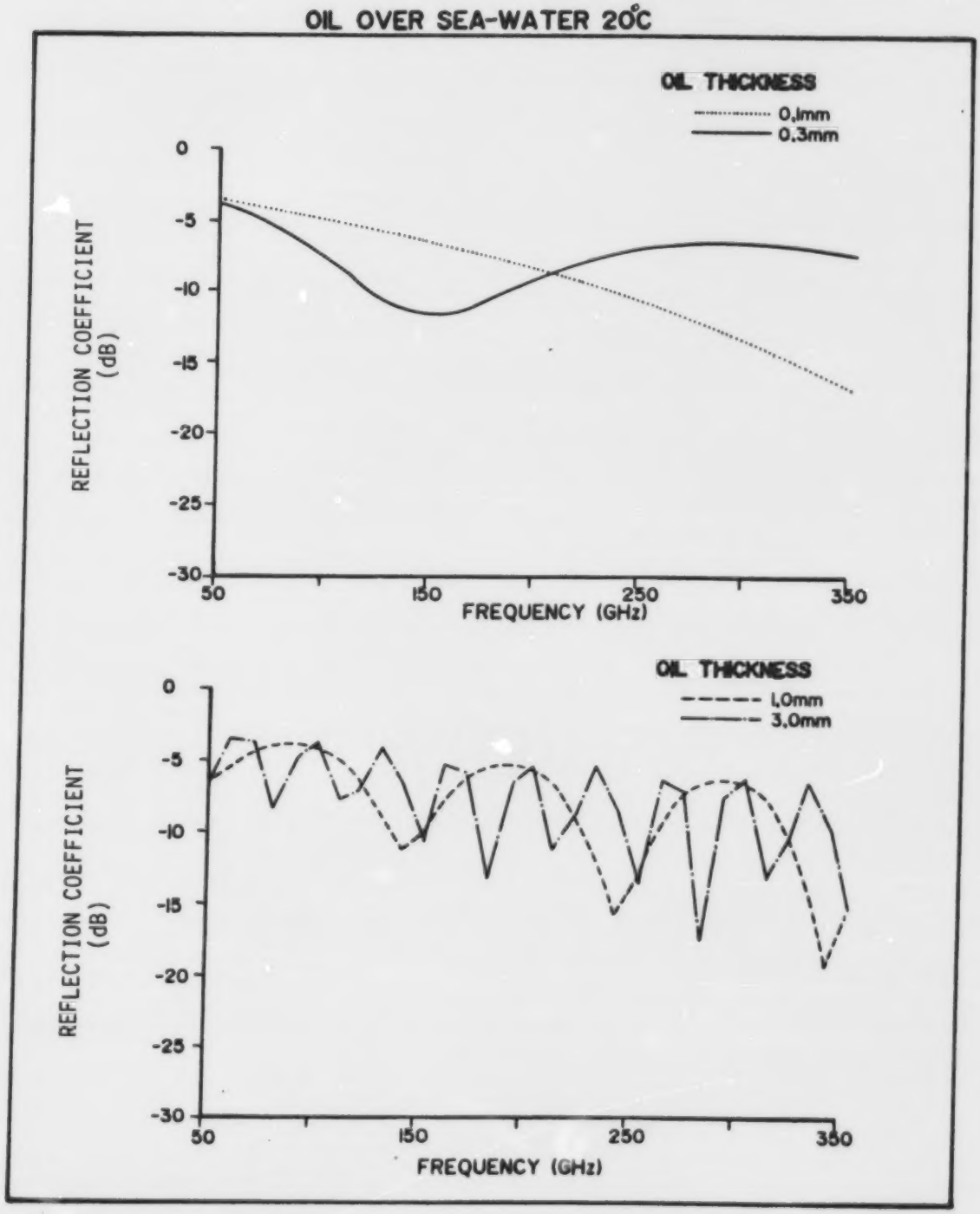

Figure 7 Calculated reflection coefficient for oil over sea-water at 20°C as a function of frequency for various thicknesses of oil layer. Dielectric constant of oil is 2.25.

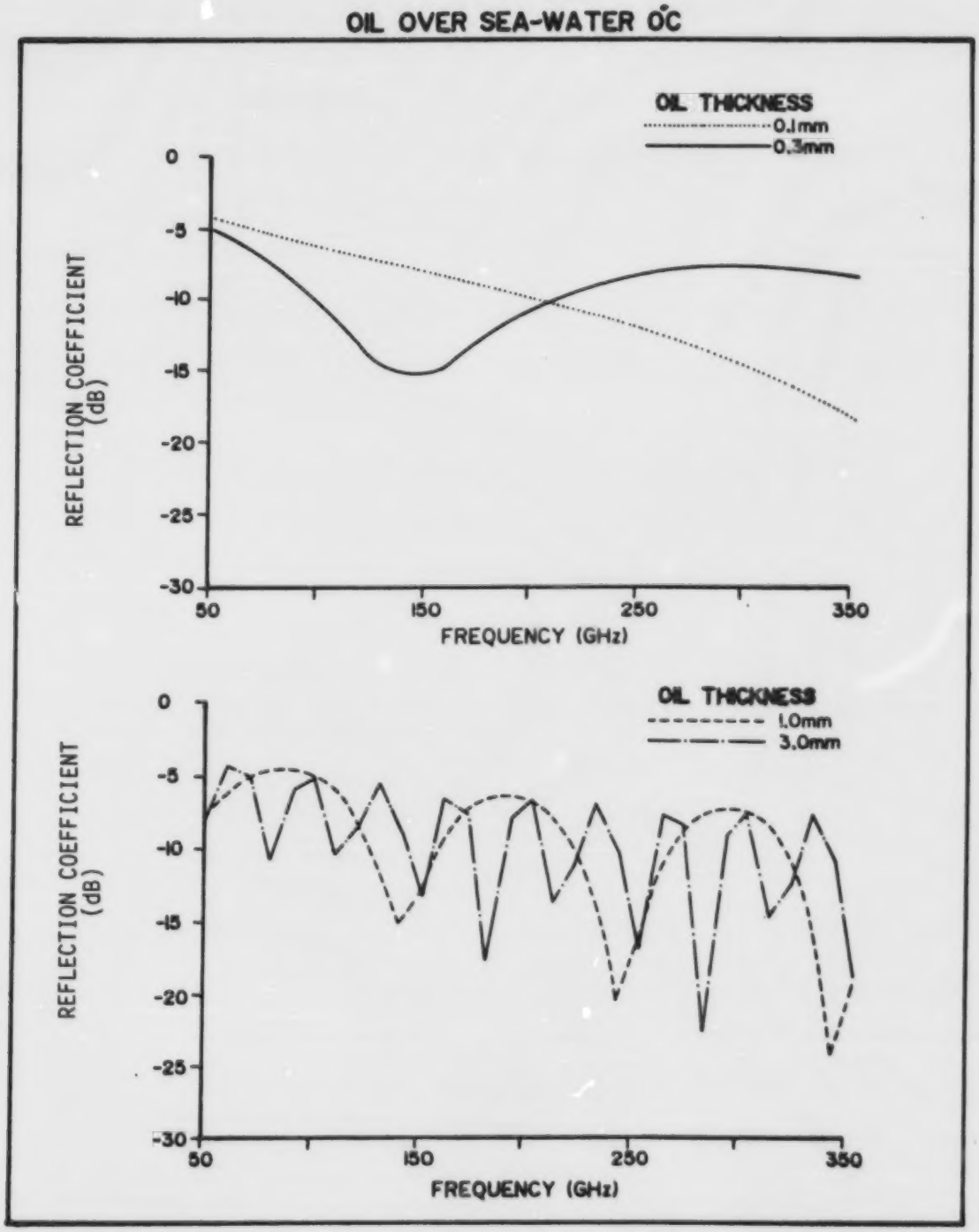

Figure 8 Calculated reflection coefficient for oil over sea-water at $0^{o}C$ as a function of frequency for various thicknesses of oil layer. Dielectric constant of oil is 2.25.

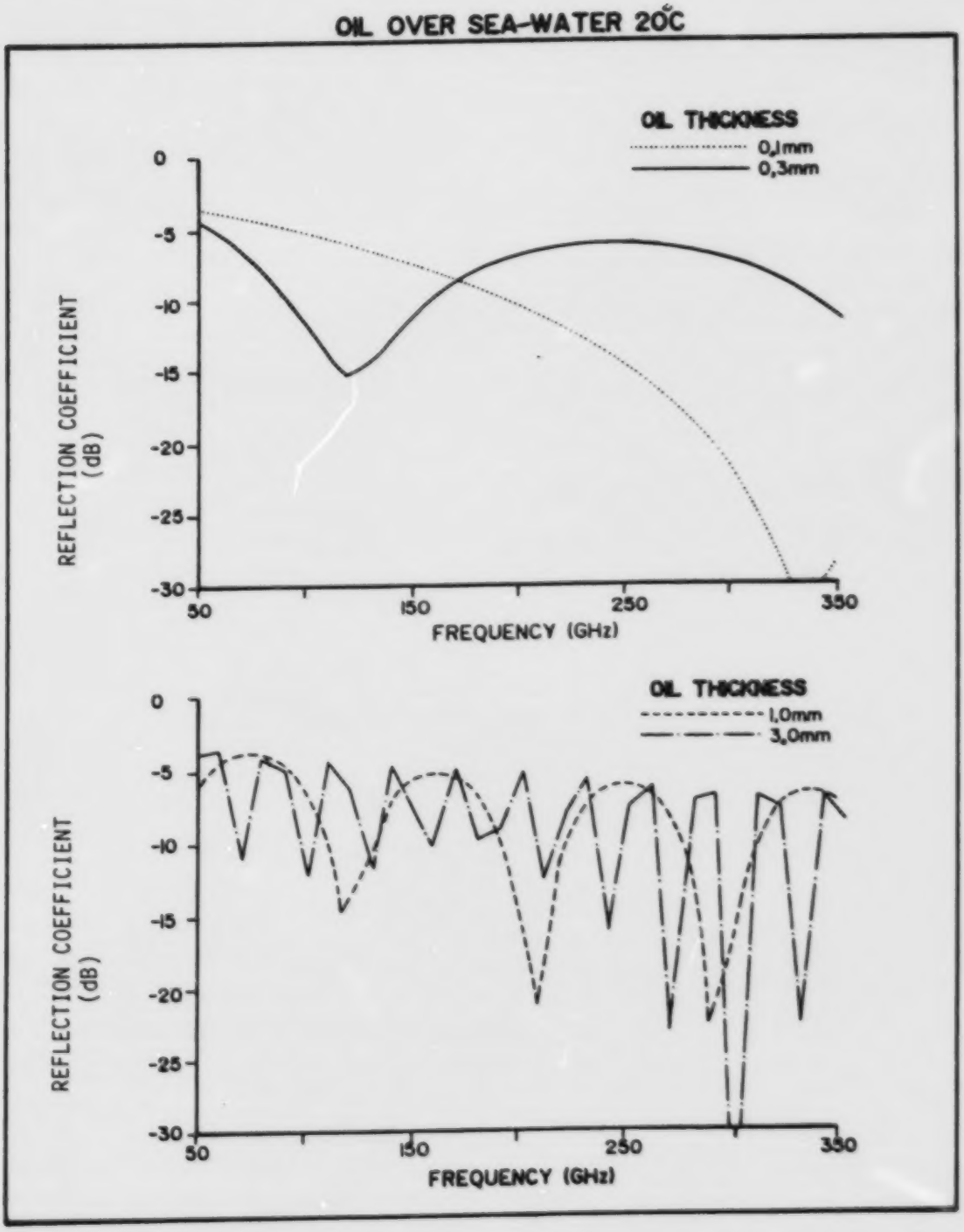

Figure 9 Calculated reflection coefficient for oil over sea-water at 20°C as a function of frequency for various thicknesses of oil layer. Dielectric constant of oil is 3.

oil. The depth of the nulls also changes because of the different matching to the water layer below. As expected from equation 2.7 the rate of beating increases slightly.

The nulls observed typically are symmetrical with frequency (when the electrical properties of the water are fairly constant). Asymmetries in the plots (Figures 5 to 9) are due to discrete sampling along the frequency axis. The calculations suggest that typical nulls for smooth, uniform layers will be 5 to 15 dB in amplitude.

The depth of nulls also is controlled by the exact position of the frequency point. Hence it is possible to miss a null by not sampling adequately in frequency. This problem is not only a theoretical one - it will also be seen in a practical situation depending on sampling in the frequency domain. If the oil layer is thick enough, the measured spectrum can be aliased, giving an incorrect thickness estimate. From equation 2.6, the sampling rate must be a few GHz if oil layers up to 30 mm thick are expected.

2.6 FOOTPRINT SIZE

The footprint on the ocean surface will be determined by the aperture of the transmitting/receiving antenna and the flying height. For a single, wide-band antenna, the radiated beamwidth will be largest at the lowest frequency. The footprint diameter,

D, will be approximately:

$$D = R \frac{3 \times 10^8}{f\ A} \text{ m} \qquad [2.8]$$

where: R is range (m)
f is radar frequency (Hz)
A is aperture size (m).

Hence, at 50 GHz a 25-cm antenna will illuminate a footprint with about 50-cm diameter at 20 m, or 2.5 m at 100-m flying height. Higher frequencies will have proportionally smaller diameter footprints.

2.7 ROUGH OCEAN SURFACE

A comprehensive discussion of the expected effects from oil on a rough ocean is beyond the scope of this report. However, in qualitative terms, several changes can be expected, both because the surface being studied is no longer planar and because the oil layer is unlikely to have a uniform thickness.

Without entering into a definition of "roughness," at frequencies above 1 GHz and near normal incidence angles, the ocean surface can be described adequately as having undulations whose size is much greater than the electromagnetic wavelength (Beckmann and Spizzichino 1963). At normal incidence the reflected signal decreases slightly as the ocean becomes rougher. Backscatter above 50 GHz is not very frequency-dependent.

The roughness of the surface is unlikely to have a serious effect on the principle of this technique, because received echoes will come primarily from ocean facets orthogonal to the incident

radar waves (shown schematically in Figure 10); i.e., specularly reflected. Although there will also be a diffuse component of reflection (Beckmann and Spizzichino 1963), it is much lower than the specular component, dropping by 5 to 15 dB at an incidence angle of 10°.

The effect of a non-uniform oil thickness probably will be that each reflecting facet may give a somewhat different interference pattern. These will be added at the receiver, so that individual nulls will be smeared. However, the sum effect will be to give broader nulls at the same radio frequencies as would be observed from an oil layer with a thickness of the average oil thickness (Figure 10). To determine an ocean backscatter intensity independent of the oil layer, a measurement could be made at a frequency low enough (e.g., 1 GHz) that the oil is a poor matching dielectric. At this frequency the oil will have a negligible contribution to the backscatter.

Therefore, although a theoretical and/or experimental evaluation is still required, it appears that ocean roughness and moderately non-uniform oil thickness will not preclude the use of this technique.

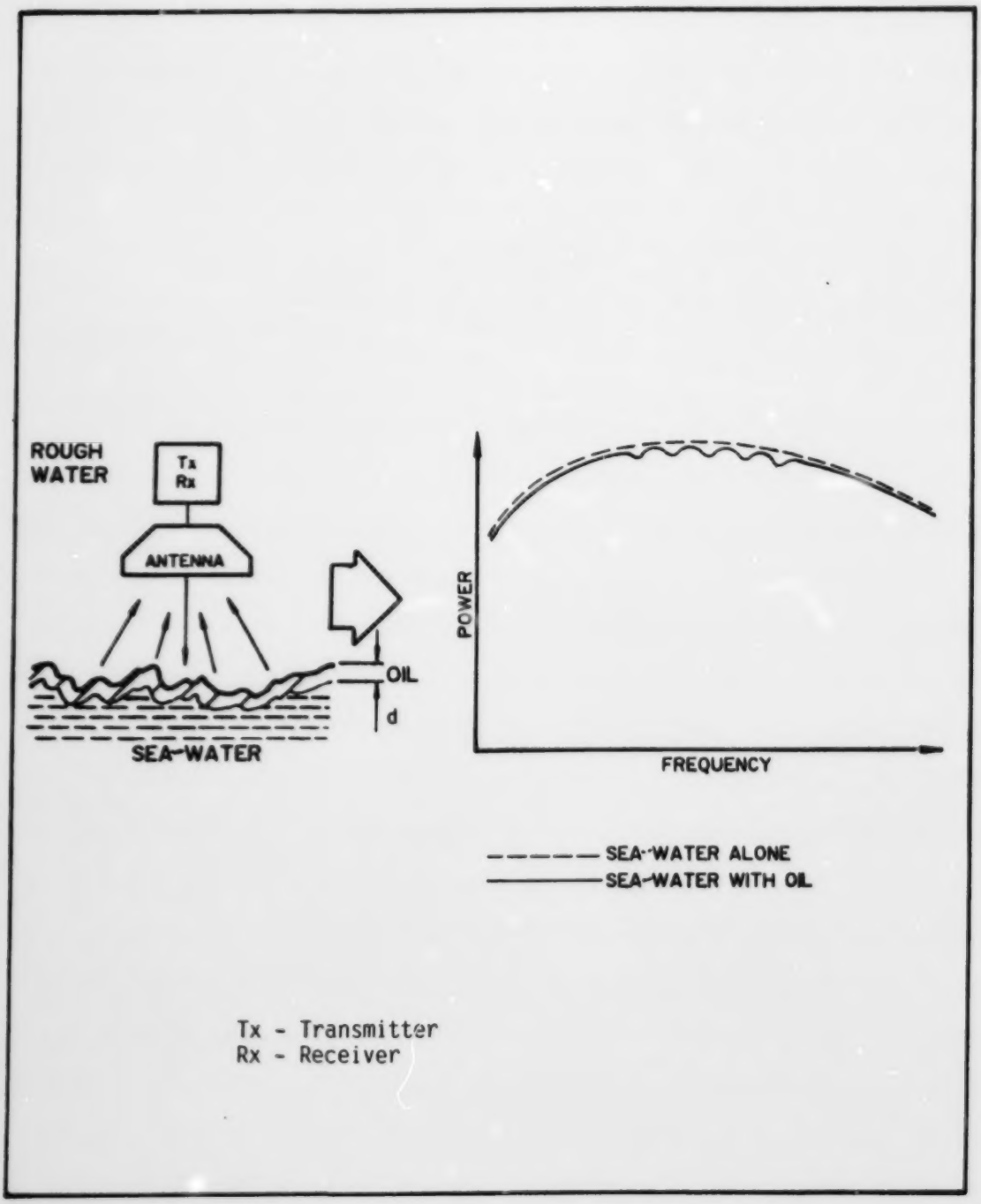

Figure 10 Sketch of active microwave spectroscopy over rough ocean

3. EXPERIMENTAL MEASUREMENTS

Measurements were made in an attempt to verify the technique experimentally. A broad-band pulse was used which was analyzed spectrally, rather than using discrete frequencies.

The specific objectives were to demonstrate:

a. The occurrence of interference transmission bands with an appropriate dielectric matching layer.

b. The practicality of detecting these bands with an impulse radar.

3.1 METHOD

The impulse radar system used in this evaluation operated at centre frequencies of about 100 to 400 MHz (wavelengths in air of 3 to 0.5 m), as opposed to the 30 to 300 GHz (wavelengths in air of 10 to 1 mm) required for an airborne system. Therefore the layer thicknesses were scaled up by a factor of about 300. The layer materials were chosen to be appropriately matched dielectrics to observe interference, i.e., $\varepsilon_2 \approx \sqrt{\varepsilon_1}$. Materials with high relative dielectric constants were used to reduce the absolute layer thicknesses required.

3.1.1 Experimental set-up

The experimental set-up is illustrated in Figure 11. A Geophysical Survey Systems Inc. (GSSI) impulse radar with bistatic 400 MHz centre-frequency antennas (Rossiter et al. 1977) was used. Water was selected as a lower layer medium, more for its high dielectric constant (81), than for realism. Published data (Morey 1974) indicate that dry silica sand has a dielectric constant of about 4 to 6, whereas wet saturated sand has a die-

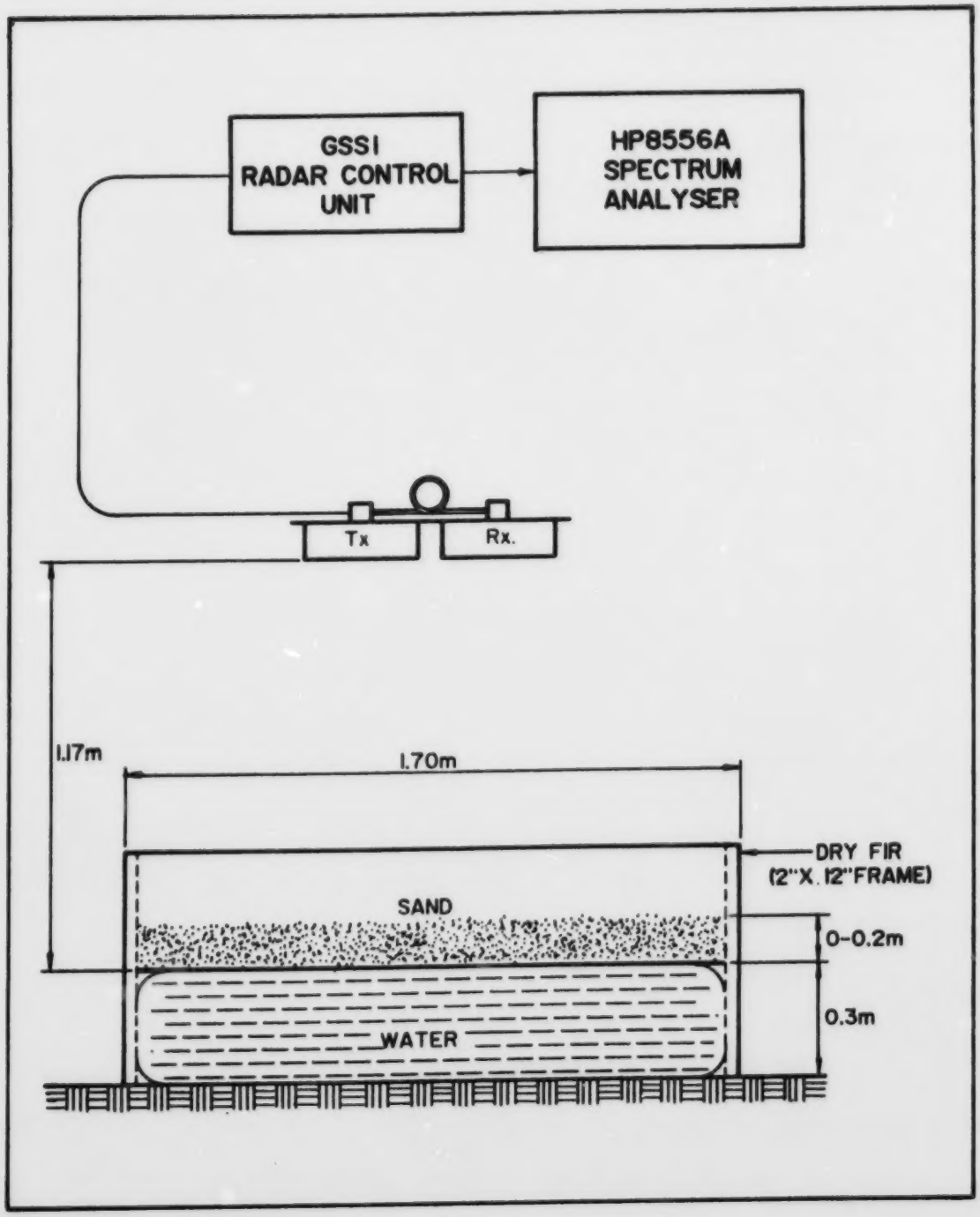

Figure 11 Experimental set-up using impulse radar system over sand and water

lectric constant of about 30. The required matching dielectric constant $\epsilon_2 = 9$ was obtained by using a sand-water mixture.

The radar output was windowed so that the surface echo pulse was the predominant signal. The demodulated radar output was then fed directly to an HP8556A spectrum analyser set up to scan over the frequency range from 0 to about 2 kHz, corresponding to a radar frequency range from 0 to 1.2 GHz. Both the radar pulse echo waveform and the spectrum analyser display were recorded on polaroid film.

The antenna to surface distance was greater than 1 m and all other nearby surfaces and objects were at greater distances. Therefore no nearfield loading of the antenna should be seen for frequencies above about 100 MHz (Mazda 1984).

3.1.2 Radar and spectrum analyser calibration

The radar window setting was fixed at the beginning of the experiment and was calibrated against a range measurement as illustrated in Figure 12 and set to about 29 ns. The demodulated pulse repetition frequency (PRF) was set at 51.2 scans/s, resulting in a demodulation conversion factor of

$(29 \times 10^{-9} \times 51.2)^{-1} = 673$ kHz per Hz.

The spectrum analyser was set up to scan from zero Hz at 200 Hz/division with a bandwidth of 10 Hz and with a vertical sensitivity of 10 dBV/division. These settings correspond to a radar equivalent scan rate in the frequency domain of 135 MHz/division.

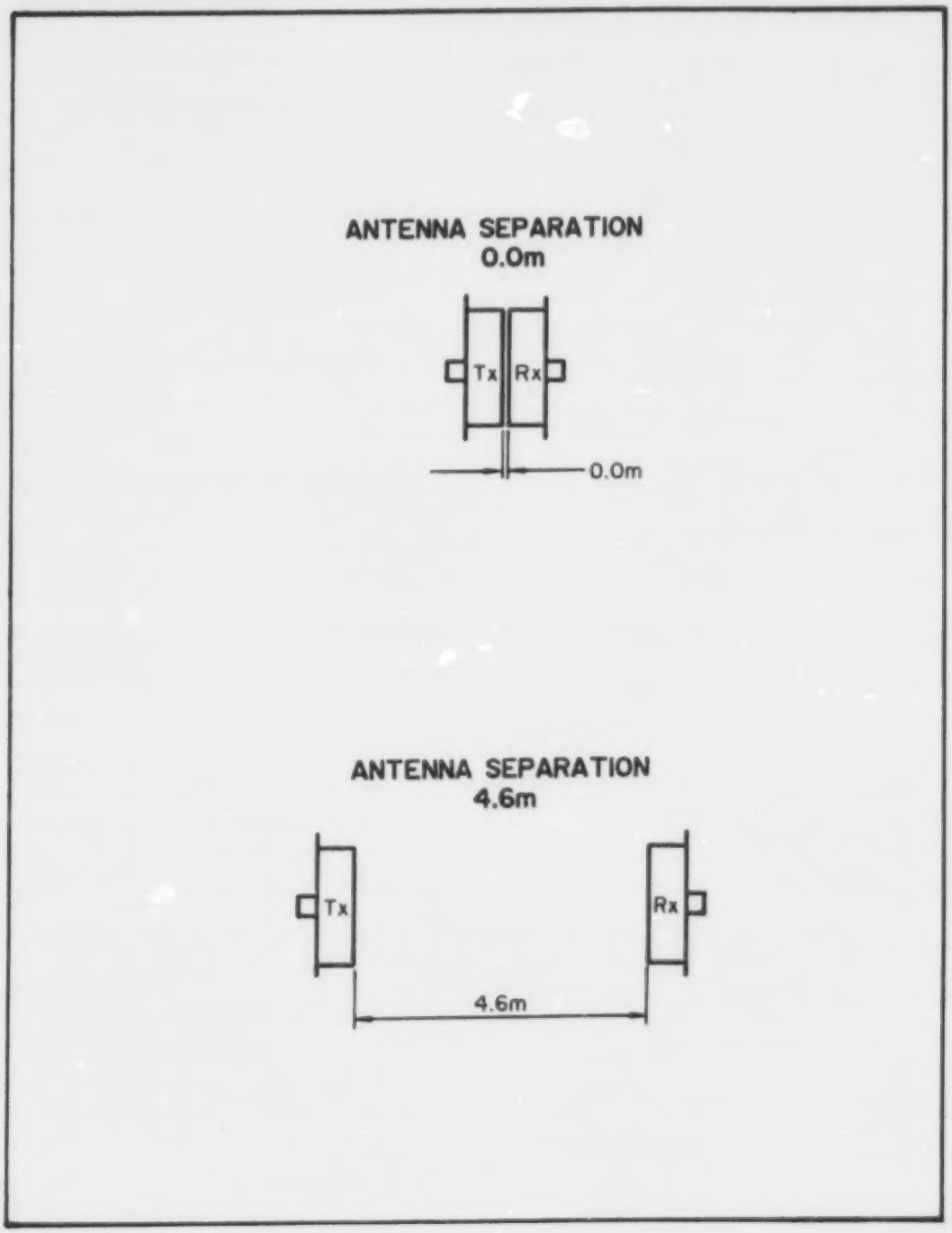

Figure 12 Radar window calibration. The radar antennas were separated by 4.6 m and the resulting delay of 15.3 ns was used to calibrate the oscilloscope trace.

3.1.3 Dielectric constant of sand

The sand used in this experiment was dry, washed, construction-grade silica. The dielectric constant was determined by measuring the radar wave velocity through 0.73 m of sand, as illustrated in Figure 13. The measured relative dielectric constant was estimated in this way to be about 9.

3.2 RESULTS

The radar noise floor generated by the radar was evaluated by setting the signal amplifier gain to zero and was found to be about -40 dBV. The primary signal that appears under these conditions on the spectrum analyser is generated by the radar scan frequency of 51.2 Hz. A "zero-base surface" spectrum was generated by the direct reflection from the water layer with no overlying sand. Values in the 100- to 600-MHz frequency range were -40 to -20 dBV.

Spectra for dry sand layers 5 to 20 cm thick were collected and the "zero-base surface" spectrum subtracted. The power reflection coefficients were determined as a function of frequency and smoothed along the frequency axis. Typical results for 5 and 14 cm thickness of sand are shown in Figures 14 and 15, together with calculated theoretical reflection coefficients for the same conditions.

Although there are nulls in the experimental results, they are only 5 to 10 dB. The calculated nulls are very deep (20 to 110 dB) because of the ideal dielectric match. Although in some cases it was possible to match the theoretical curves to the

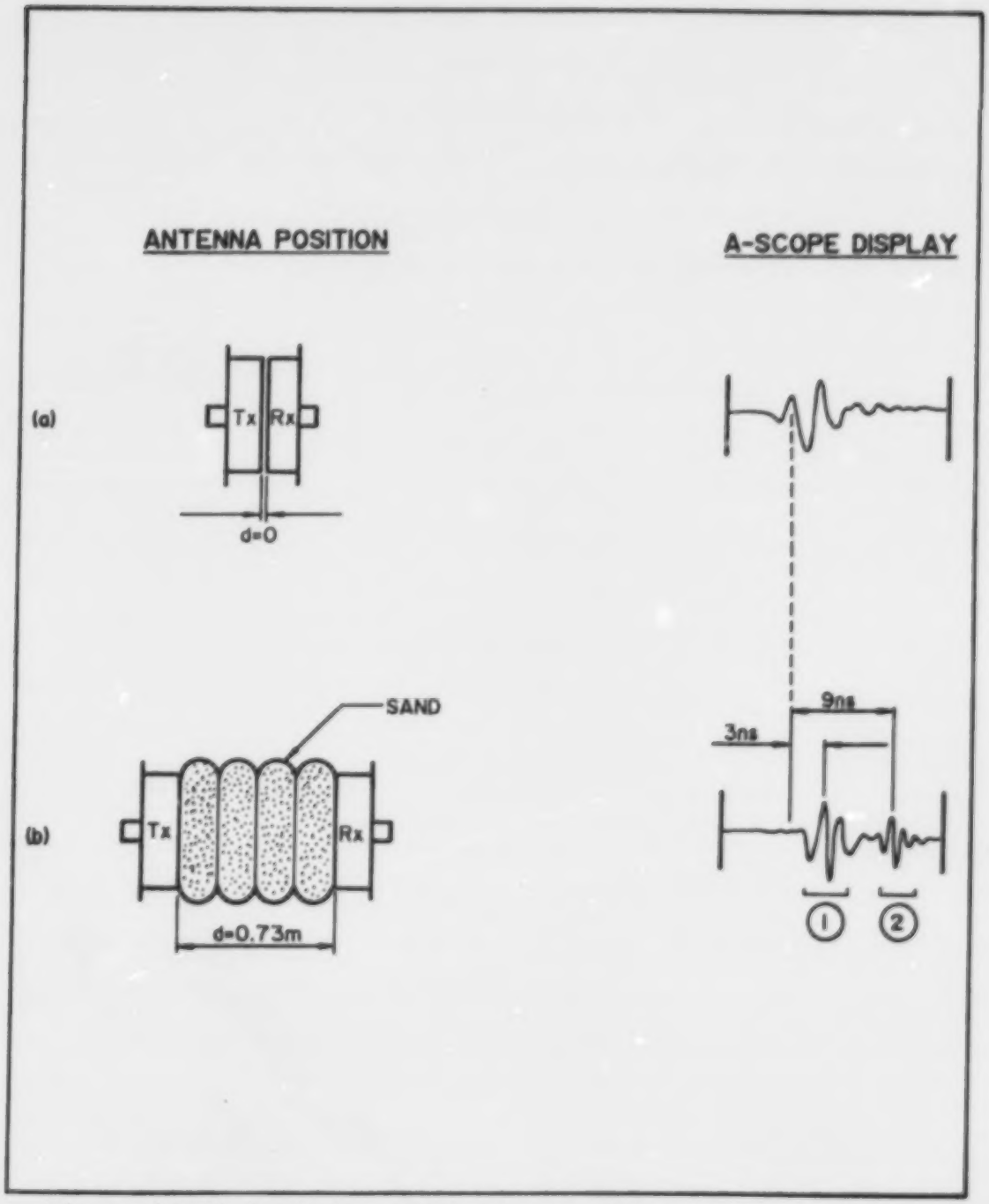

Figure 13 Dielectric constant of sand: (a) received echo for separation of 0 m; (b) received echo with 0.73 m of sand between the antennas. Pulse (1) arrives through the air (3 ns), while pulse (2) travels through the sand (9 ns). The estimated dielectric constant of the sand is thus $(9/3)2 = 9$.

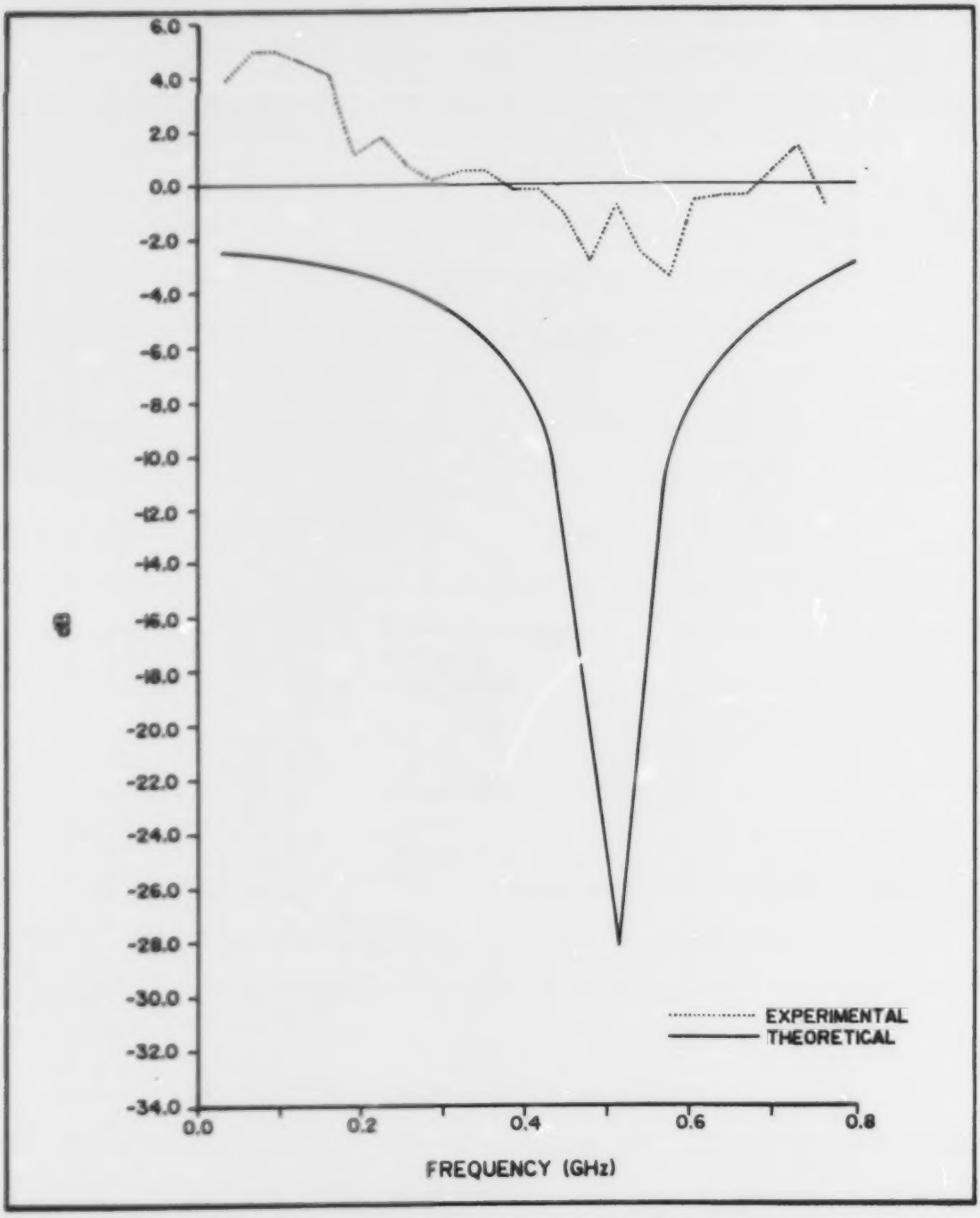

Figure 14 Reflection coefficient for 5 cm sand layer over water as a function of frequency: (a) experimental results; (b) calculated theoretical results.

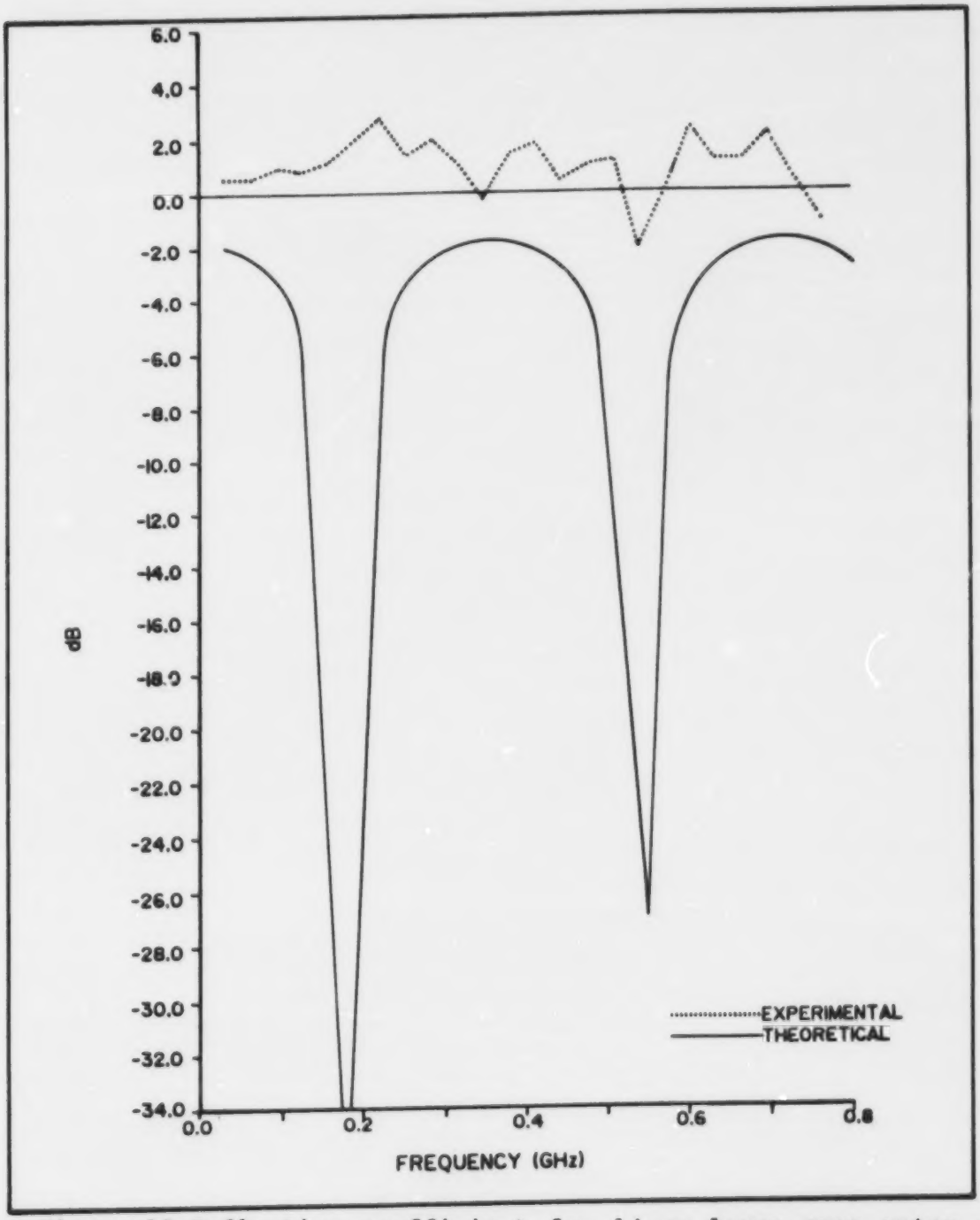

Figure 15 Reflection coefficient for 14-cm layer over water as a function of frequency: (a) experimental results; (b) calculated theoretical results.

experimental results (Figure 14), it was not possible to find a satisfying match for most of the experimental results (e.g., Figure 15). Therefore, the results of this experiment did not confirm the theory satisfactorily.

3.3 DISCUSSION

Several factors in the radar, the spectral analysis, and the broadband technique used explain the inconclusive results that were obtained.

3.3.1 Radar pulse characteristics

Interference phenomena for short broad band pulses will be dependent on the phase and amplitude of the interfering pulse. Hence, the actual shape of the GSSI impulse radar output pulse is an important factor in predicting the possible interference patterns in the received pulse.

Butt and Gamberg (1979) measured GSSI output characteristics, as shown in Figure 16. While the transmitter output into a resistive load is close to an ideal pulse, the shape of the pulse is distorted by both the transmit and receive antennas. The best approximation to the pulse transformation by each of the transmit and receive antennas is a differentiation. Thus the actual shape of the transmitted pulse is the differential of Figure 16(a) or the integral of Figure 16(b).

The Fourier tansform, F, of the nth derivative of a function is obtained by multiplying F by a term in f^n, where f is frequency (Weaver 1983). Thus the power spectrum of the derivative will be shifted toward higher frequencies but will show the same basic

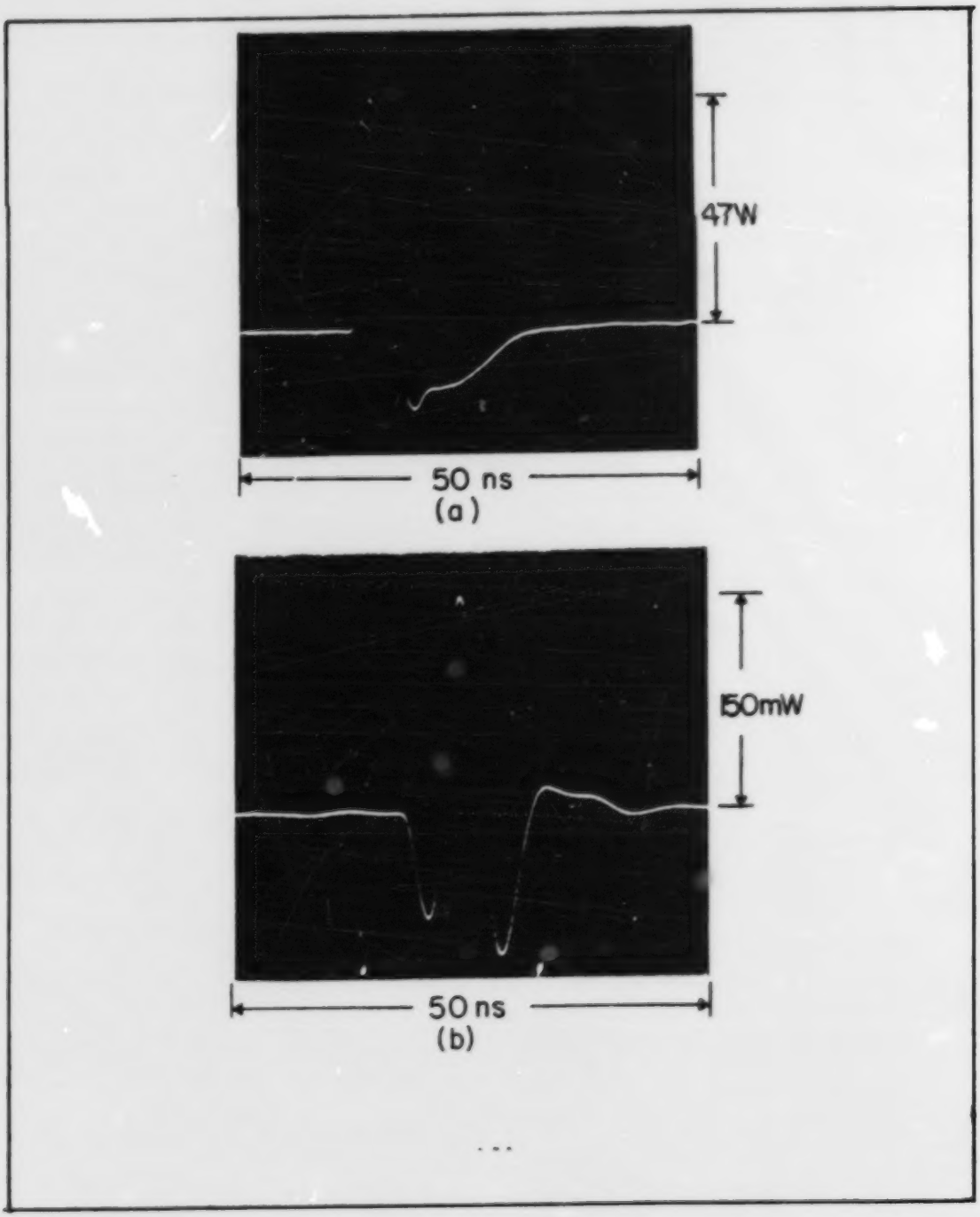

Figure 16 Impulse transmitter output pulse: (a) into a 200 Ω resistive load; (b) into antenna coupled through a 200 to 50 Ω wideband balun to a 50 Ω input sampling oscilloscope.

lobes and zero crossings. Therefore, incorporation of this term will change the spectrum by a factor of f, but will not account for some of the observed nulls in the measured spectra.

3.3.2 Spectral analysis of the radar output

The experimental set-up for real-time spectral analysis of the GSSI output presents the power spectrum for a received pulse added to a fundamental repetition rate of 51.2 scans/s. The resultant spectrum will not be equivalent to the analysis of a single windowed pulse. Any shift in the position of the echo pulse in the scan will shift a set of interference patterns in the spectrum analyzer based on the fundamental frequency of the pulse trains.

It appears that this mechanism could explain the observed spectra because of interference mechanisms "internal" to the analysis routine. To obtain meaningful results, a single stationary window should have been used.

3.3.3 Pulse-length limitations

For the experiment here the pulse length was about 3 ns. Two-way travel speed in a medium with a dielectric constant of 9 is 5 cm/ns; therefore only layers of less than 15 cm would show any interference nulls.

There is a fundamental inconsistency in using a short pulse to provide a wide bandwidth source in order to examine frequency-dependent interference effects. As the interferences to be observed depend on a continuous wave signal, they will be non-existent when the two-way travel-time in the upper layer is

greater than the pulse length.

3.3.4 Summary and conclusions

The experimental attempt to demonstrate interference phenomena using impulse radar reflections from matched-layered media had serious flaws. Before this experimental work took place, it was postulated that a broadband pulse could be used to generate the required signal for this technique. As shown above, this approach is not adequate, except possibly for thin layers. Therefore discrete frequency signal generation is required. Recommended experimental procedures are given in Chapter 4.

4. DISCUSSION AND RECOMMENDATIONS

4.1 CONCLUSIONS

On the basis of relatively straightforward plane-layer theory, active microwave spectroscopy appears capable of estimating the thickness of oil slicks on water with thicknesses from 0.1 to about 30 mm. Observed nulls appear theoretically to be 5 to 15 dB in amplitude for smooth layers. Oil thickness range will be determined by the highest radar frequency used and by the sampling in radar frequency. Undersampling could lead to ambiguous results because of aliasing. Footprint size would probably be in the order of meters. Effects of rough oceans are not yet determined, but might not be severe.

Simple wide-band pulse experimental results were unable to verify the theory adequately due to the experimental procedures used. However, a discrete-frequency system that covered the required frequency range appears attractive for this application. Engineers at the University of Toronto have developed a wide-band stepped-frequency radar for ground probing applications (Iizuka and Freundorfer 1983). Millimetre-wave sources are built by Hughes Aircraft and appropriate frequency-steppers and wide-band antennas (DuHamel and Chadwick 1984) are available.

4.2 RECOMMENDATIONS FOR FURTHER WORK

An experiment is recommended using a discrete-frequency system. The experiment should have the following objectives:

a. To verify the plane-layer theory described in this report.

b. To measure the response from rough surfaces and non-uniform layers.

c. To determine operational parameters for a practical system, such as source and receiver configuration, height above the oil/water, recording and data reduction requirements, cost, etc.

The experiment should be conducted in a test basin several meters wide, i.e., large enough to place the transmitter and receiver several tens of meters above the surface without illuminating the basin walls. However, it should be small enough to constrain the amount of oil required, and it should have a wave generating apparatus. A source (or sources) capable of generating microwave frequencies over the 50 to 300 GHz range and of being stepped through a pre-programmed set of frequencies will be required, together with a wide-band antenna such as a horn, appropriate receivers, recording apparatus and calibration equipment.

The primary observations will be return signal level as a function of frequency for a variety of experimental conditions, such as:

- oil thickness
- wave generation
- non-uniform oil
- antenna height
- oil viscosity
- off-nadir look angles.

Data analysis should concentrate on identifying the problems involved in implementation of a practical system. Hence, the experiment should provide information needed to estimate the costs of assembling a working system.

This experiment is estimated to cost about $50,000 to $100,000, depending on the availability of a suitable test tank. It is expected that two or three weeks of experimental work would be required at the tank once the components had been assembled. The experimental work could also be combined with testing another technique, electromagnetic thermoelastic emission, described in Part B of this report.

B. ELECTROMAGNETIC THERMOELASTIC EMISSION

1. INTRODUCTION

1.1 BACKGROUND

The absorption of electromagnetic wave energy in a transmitting medium can give rise to elastic waves as a result of spatial or time variations in energy deposition. Localized heating causes differential thermal expansion. Both thermal waves and elastic stress waves (acoustic waves) are generated if there is a spatial or temporal discontinuity.

The efficiency of conversion, N, of electromagnetic to elastic waves is low: in the order of $N = 10\text{-}12\ I_o$ to $10^{-16}\ I_o$, where I_o is the incident power, for unconfined liquids and gases at atmospheric pressure. Much of the initial research in this field has involved high-energy laser pulses and surface heating effects (Gournay 1966; White 1963). Explosive surface ablation by a high-energy pulse is not significantly more efficient than the thermoelastic effects that generate acoustic waves at lower incident energy levels (Scruby 1986). Thermoelastic effects are similar whether the irradiation takes place at microwave, visible or X-ray frequencies. The only fundamental requirement is for anisotropic energy absorption in the target material.

Applications of thermoelastic effects include photo-acoustic spectroscopy as a very sensitive analytical tool for trace detection in gases and liquids (West et al. 1983). Photo-acoustic spectroscopy generally involves use of modulated laser sources irradiating confined samples and use of a microphone to

detect acoustic signals.

Low-energy microwave-thermoelastic phenomena are currently being investigated as potential biomedical imaging technologies (Lin and Chan 1984). Microwave irradiation intensities in the order of 10 kW/m^2 peak power can generate detectable thermoelastic effects related to differences in electromagnetic impedance between organs and other types of tissue. This same phenomenon gives rise to microwave auditory effects (Lin 1977; Borth and Cain 1977). Humans and animals irradiated by microwave pulses can "hear" the pulse via a thermoelastic conversion mechanism.

A third application is remote non-destructive testing of materials such as steel billets during hot rolling operations (Monchalin 1985b). This application is similar to the oilspill film thickness measurement problem. The techniques that have been developed for both irradiation and detection are largely applicable to the problem addressed in this report, in that they are suited for non-contact measurements of thickness in an acoustically noisy environment.

1.2 OUTLINE OF REPORT

The objective of this study is to evaluate the feasibility of using a radiation-induced thermoelastic pulse for remote, airborne measurement of oil slicks with thicknesses ranging from about 0.1 to 10 mm.

A theoretical estimate of the magnitude of thermoelastic effects, oil film acoustic signatures, and an investigation of the range and sensitivity of several possible detectors is given

in Chapter 2. Experimental verification is given in Chapter 3 and a possible system design is described in Chapter 4, together with recommendations for further work.

2. THEORETICAL FEASIBILITY

Feasibility of the thermoelastic technique was assessed by examining the magnitude of the major physical effects. Questions to be addressed included:

a. Can a conventional laser or microwave source deliver enough energy from a minimum range of 20 m (altitude of aircraft) to generate a detectable acoustic wave?

b. Will an oil film on sea-water display a unique acoustic signature?

c. Can the acoustic behaviour of the film be detected using existing sensors?

2.1 IRRADIATION TECHNIQUES

Practical irradiation sources that could be operated from a helicopter or light aircraft include visible or infra-red (IR) lasers and radar transmitters. Table 1 summarizes the peak power intensities and wavelengths of several compact off-the-shelf sources.

The absorption characteristics of the target medium and the subsequent thermoelastic pulse will be sensitive to the wavelength of the electromagnetic irradiation source. Signals from a laser source operating in the visible or near IR will be strongly attenuated in the oil layer, depending on chemical composition and film thickness, while attenuation in water will be low. For a 10-um laser, most of the energy will be absorbed within a few hundred micrometres thickness of oil or water. On the other hand, for a 10-GHz microwave continuous wave (cw) pulse, little

Table 1

Typical irradiation sources

(based on commercial product literature)

Source	Wavelength	Peak power	Pulse duration	Beam divergence
Nd:Yag Laser	1 um	10 MW	8 ns 10 per second	0.5 mrad
CO_2 Laser	10 um	100 W	modulated cw	6.5 mrad
X-Band Radar	3 cm	25 kW	modulated cw	17 mrad (1^o)

energy will be absorbed by the oil layer, and the underlying water layer will absorb most of the energy within a few millimetres of its surface. In each of the cases both the thermoelastic pulse generation mechanism and the response signature of the oil film will be different.

2.2 THERMOELASTIC RESPONSE

The generation of elastic or acoustic waves in an absorbing medium is a result of elastic stress associated with induced temperature gradients. Gournay (1966) reported a series of analytical expressions for free and constrained liquid media including two-layer situations similar to an oil slick over water. Gournay also performed experimental work that confirmed the analytical results. Note that for these calculations and for all of the situations considered in this study, the analysis is for a one-dimensional situation in which the diameter of the irradiated area is assumed to be much larger than the depth of the heating effects.

The expression for efficiency of electromagnetic to acoustic energy conversion is:

$$N = \frac{E_a}{E_e} = 5\, I_o \left[\frac{C\,\beta^2}{\rho\, S^2\, Q^2}\right] F(\alpha CT) \qquad [2.1]$$

where, E_a is the acoustic response, E_e is the irradiation power, and

$$F(\alpha CT) = \frac{1 - e^{-\alpha CT} - \alpha CT\, e^{-\alpha CT}}{\alpha CT} \qquad [2.2]$$

for a free liquid surface (symbols and units are defined in Table 2). For a constrained liquid surface, i.e., a liquid surface with an overlying layer of another liquid,

$$F(\alpha CT) = \frac{\alpha CT\, e^{-\alpha CT} + 3e^{-\alpha CT} + 2\alpha CT - 3}{\alpha CT} . \qquad [2.3]$$

The value of $F(\alpha CT)$ for a free liquid and has a maximum value of 0.3 when

$$\alpha CT = 2 \qquad [2.4]$$

i.e., when the electromagnetic absorption length α , or "skin depth" approximately matches the acoustic pulse length, CT. For a constrained liquid, $F(\alpha CT)$ approaches a limiting value of 2 for relatively long acoustic pulse lengths; i.e.,

$$\alpha CT >> 1. \qquad [2.5]$$

Examination of the expression for conversion efficiency indicates that the efficiencies are low but also that they are proportional to the incident power levels, I_o. This property means that thermoelastic pulse energy will increase as the square of electromagnetic pulse energy. The equations are valid for energy intensity levels that do not induce phase changes in the liquid. For oil and water the equations can be considered valid at delivered energy densities of less than about 60 MJ/m^3.

Table 2

Symbols and units for acoustic response

Symbol	Meaning	Units
N	Thermoelastic conversion efficiency	
E_a	Acoustic energy	J
E_e	Electromagnetic irradiation energy	J
I_o	irradiation power	W/m^2
C	velocity of sound	m/s
β	coefficient of thermal expansion	$^oC^{-1}$
ρ	density	kg/m^3
S	specific heat	$cal/(kg \cdot ^oC)$
Q	mechanical equivalent of heat	J/cal
a	attenuation rate	m^{-1}
T	irradiation pulse length	s

$F(aCT)$ is defined in the text for free and constrained surfaces.

Conversion efficiency values for water and oil (see Tables 3 to 5) under optimal pulse length conditions are in the order of 10^{-15} I_o. Thus for incident energy levels of 10 kW/m^2 the acoustic energy levels will be in the order of 10^{-11} W/m^2.

The physical displacement, Δx , associated with the energy absorbed can be derived from Love's stress-strain relationship (Gournay 1966) for a heated medium. Displacement is shown in Appendix A to be approximately:

$$\Delta x \approx \frac{\beta I_o T}{\rho Q S} . \qquad [2.6]$$

This expression is valid for situations where the characteristic attenuation length is small compared to the irradiated surface dimensions and where inertial confinement effects are small. For the oil and water media under consideration equation 2.6 is valid to the first order.

The three irradiation sources considered in Section 2.1 will result in different characteristic responses from an oil film on water. The three-layer geometry is illustrated in Figure 17. Using the approximate values for C, β, S, ρ, and N listed in Tables 3, 4, and 5, an approximate response can be characterized for each type of source, as summarized in Table 6. Note that these are order of magnitude estimates only!

2.2.1 Nd:Yag Laser

Pulsed infra-red lasers are available with peak powers of 10 MW and pulse lengths of 8 ns, giving electromagnetic energies

Table 3

Physical properties of liquids

	C Velocity of Sound (m/s)	β Expansion Coefficient ($^oC^{-1}$)	S Specific Heat (cal/(kg·^oC) x 10^3)	ρ Density (kg/m^3 x 10^3)
Water	1.5×10^3	6.9×10^{-5}	1.0	1.0
Sea-water	1.5×10^3	4.1×10^{-5}	1.0	1.0
"Oil"	1.3×10^3	1.0×10^{-4}	0.25	0.8

Table 4

Attenuation rate (α) vs wavelength for oil and sea-water (m^{-1})

Wavelength	Oil	Sea-water
500 nm - 1000 nm	10^3	1
10 um	$\sim 10^4$	10^5
3 cm	<10	10^3

Table 5

Thermoelastic conversion efficiency
(based on Tables 3 and 4)

Medium	$N / I_o F(\alpha CT)$
Sea-water	7.1×10^{-16}
Oil	7.4×10^{-14}

Maximum $F(\alpha CT)$ = 0.3 free liquid for $\alpha CT = 2$,
= 2 constrained liquid for $\alpha CT >> 1$.

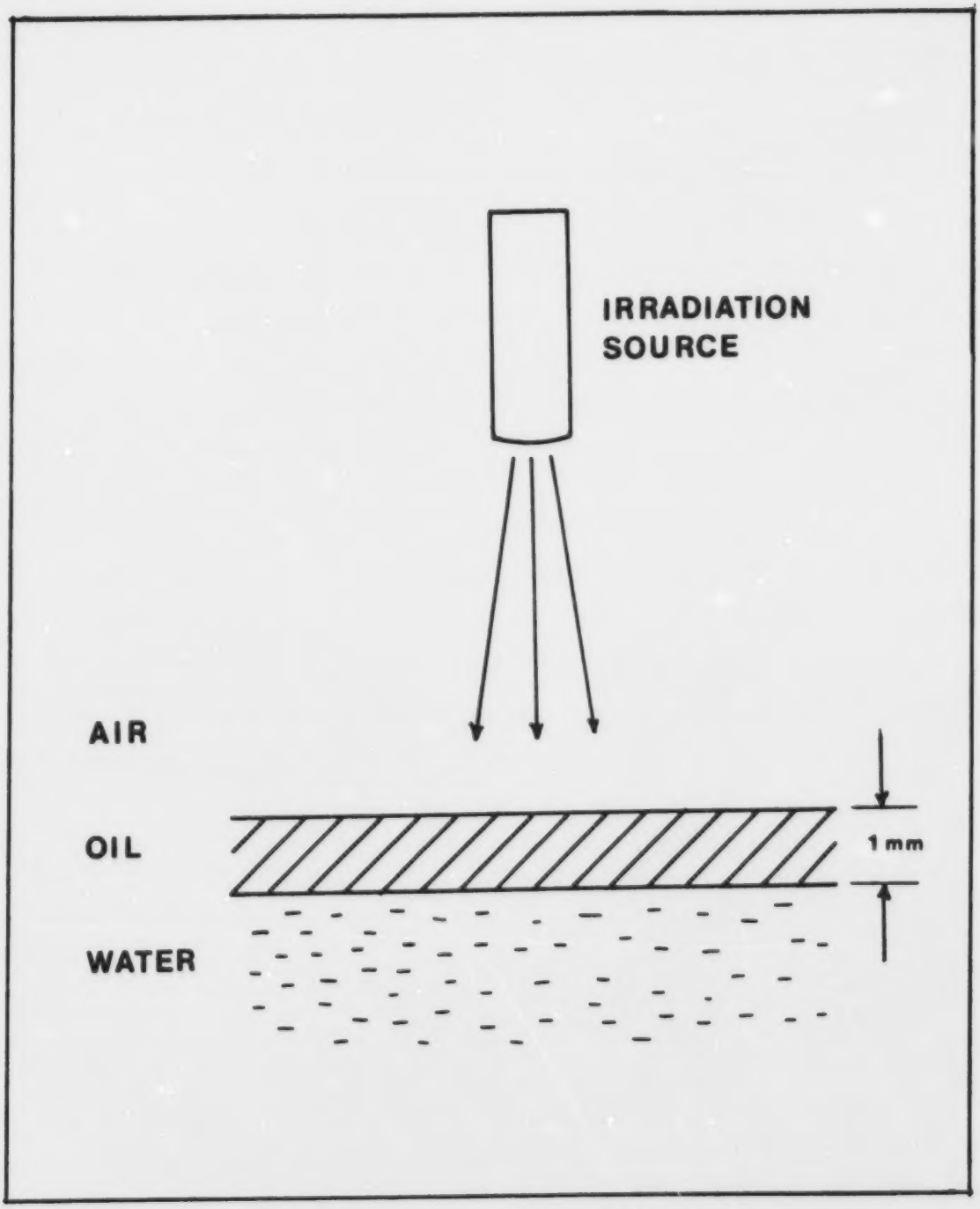

Figure 17 Geometry of electromagnetic thermoelastic source irradiating an oil layer on water

Table 6

Approximate acoustic power and mechanical displacement for three sources described in Table 1

Source	Nd:Yag laser	CO_2 laser	X-band radar
Peak EM power (W)	1×10^{7}	100	25×10^{3}
Area illuminated at 20 m (m^2)	1×10^{-3}	1×10^{-2}	2.5
Peak EM intensity at 20 m, I_o (W/m^2)	1×10^{10}	1×10^{4}	1×10^{4}
Pulse length, T (s)	8×10^{-9}	1.5×10^{-7}	1×10^{-6}
Acoustic speed C (m/s)	1.3×10^{3} (oil)	1.3×10^{3} (oil)	1.5×10^{3} (water)
Acoustic attenuation, (m^{-1})	1×10^{3} (oil @ 1 um wavelength)	1×10^{4} (oil @ 10 um)	1×10^{3} (water at 3 cm)
αCT	1×10^{-2}	2	1.5
F(αCT)	5×10^{-3} (free liquid)	0.3 (free liquid)	0.7 (constrained liquid)
Conversion efficiency, N	3.7×10^{-6}	2×10^{-10}	5×10^{-12}
EM energy/pulse, E_e (J)	8×10^{-2}	1.5×10^{-5}	2.5×10^{-2}
Acoustic energy/pulse, E_a (J)	3×10^{-7}	3×10^{-15}	1×10^{-13}
Pulse repetition frequency, PRF (Hz)	10	1×10^{6}	1×10^{5}
Average acoustic power (W)	3×10^{-6}	3×10^{-9}	1×10^{-8}
dB re: 1 uPa	116	86	92
Displacement (m)	1×10^{-8}	2×10^{-13}	2×10^{-13}

of 80 mJ per pulse. The beam can be tightly focused, but to allow for finite aperture and non-ideal optics, the effective area at 20-m range has been conservatively set at 1×10^{-3} m^2, giving a peak intensity of 10 GW/m^2.

At 1 um wavelength the electromagnetic energy will to a large extent be absorbed in the oil. Using typical properties for oil, this pulse length is poorly optimised for maximum conversion efficiency. Average acoustic power is 3.7×10^{-6} W or 116 dB re: 1 uPa. The mechanical displacement is about 10 nm.

2.2.2 CO_2 laser

This source is a relatively low-power 100-W modulated CW laser operating at a wavelength of 10 um. Again the energy will largely be absorbed in the oil. Using a beamwidth of about 6.5 mradians, the illuminated area at 20 m range is 1×10^{-2} m^2, giving a peak intensity of 10 kW/m^2. Using an optimum pulse length of 0.15 us, the maximum conversion efficiency for a free liquid surface is obtained, i.e., 2×10^{-10}.

Operating at PRF of 1 MHz, this device would give an average acoustic power of 3×10^{-9} W or 86 dB. The mechanical displacement would be about 0.2 pm.

2.2.3 X-band radar

Radars operating at 3-cm wavelength with 25 kw peak power are readily available. To obtain a reasonable beamwidth the aperture will be about 2.5 m^2, giving a peak intensity of 10 kW/m^2.

At this frequency the oil essentially will be transparent and most of the energy will be absorbed in the underlying water. For

a 1-us pulse length the conversion efficiency in water for a constrained surface will be non-optimum by factor of about 3. Conversion efficiency will be 5×10^{-12}.

With a PRF of 100 kHz (10% duty cycle), the average acoustic power will be 10^{-8} W or 92 dB. Mechanical displacement will be 0.2 pm.

2.3 ACOUSTIC BEHAVIOUR OF OIL FILMS

2.3.1 Acoustic characteristics

Once stimulated, the acoustic response of the oil layer will be determined mainly by the resonant frequency of the oil. The frequency and magnitude of the resonant response are determined largely by the layer thickness, the velocity of sound in the oil, the attenuation losses, and the reflection/transmission characteristics of the oil-air and oil-water interfaces. The velocity and attenuation of sound in crude oil depend on its chemical composition, temperature, density and weathering. Reported values for sound velocity in hydrocarbon liquids are in the range of 1,000 to 1,500 m/s; attenuation rates vary from 0.03 to 35 dB/m at 1 MHz and increase with the square of the frequency (see Table 7). These values are probably similar for crude oil (Jones and Yeatman 1985; Jones and Kwan 1983).

Table 7

Sound velocity and attenuation in various liquids

(after Blitz 1967)

Liquid	Velocity (m-1)	Viscous relaxation time (s)	Viscous absorption (neper/cm)	Attenuation at 1 MHz (dB/m)
Acetone	1,200	3.8×10^{-13}	6.3×10^{-17}	0.03
Benzene	1,320	5.6×10^{-13}	8.4×10^{-17}	0.04
Carbon tetrachloride	950	9.2×10^{-13}	2.0×10^{-16}	0.09
Castor oil	1,500	6.2×10^{-10}	8.1×10^{-14}	35
Chlorobenzene	1,320	6.8×10^{-13}	1.0×10^{-16}	0.04
Ethyl alcohol	1,200	1.7×10^{-12}	2.9×10^{-16}	0.01
Glycerol (pure)	1,940	4.2×10^{-10}	5.7×10^{-14}	25
Methyl alcohol	1,120	7.9×10^{-13}	1.4×10^{-16}	0.06
Nitrobenzene	1,480	1.1×10^{-12}	1.4×10^{-15}	0.06
Olive oil	1.440	6.0×10^{-11}	8.2×10^{-16}	3.6
Toluene	1,320	5.2×10^{-13}	7.7×10^{-17}	0.03

Reverberation frequency is determined by:

$$f = V/2t \qquad [2.7]$$

where f = the reverberation frequency, Hz

v = the sound velocity in the oil layer, m/s

t = the oil layer thickness, m.

Calculated reverberation frequencies versus an appropriate range of film thickness are shown in Figure 18 for a velocity of 1.3 x 103 m/s.

Reverberation amplitude is affected by reflection attenuation losses. Attenuation losses even as high as 100 dB/m will result in low damping for thin oil layers. Reflection at the air-oil interface will be almost perfect. However, reflection at the oil-water interface will be lossy because the acoustic impedance of the two fluids is closely matched. The power reflection coefficient, u, can be calculated:

$$u = \left[\frac{r_w - r_o}{r_w + r_o}\right]^2 \qquad [2.8]$$

where r_w, r_o are the characteristic impedances of water and oil respectively;

i.e.,

$r_w = 1.5 \times 10^6$ kg/(m^{-2}.s),

$r_o = 1.04 \times 10^6$ kg/(m^{-2}.s),

giving u = 0.03 or -15 dB.

Therefore oil film reverberation will be damped rapidly by losses at the oil-water interface.

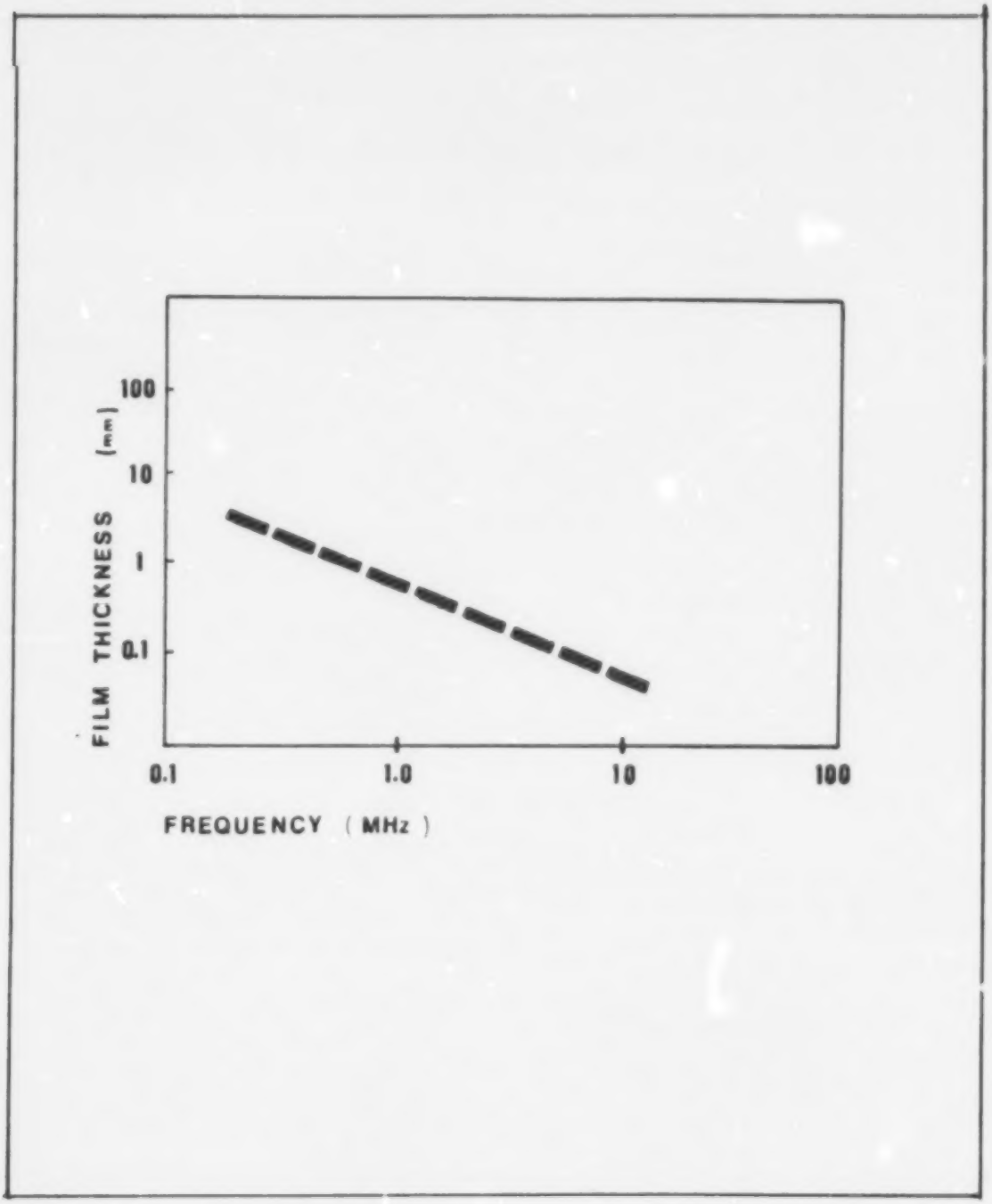

Figure 18 Calculated oil layer thickness vs. acoustic reverberation frequency, for a sound velocity of 1,300 m/s

2.3.2 Expected response

The results from the previous section can be used to estimate the response from the sources described in Sections 2.1 and 2.2.

A single, high-power laser pulse will create an acoustic pulse that will reverberate within the oil layer. The amplitude of each subsequent reflection at the oil-water interface will be about 15 dB below the previous echo, as shown in Figure 19. The time delay between echoes will depend on the thickness of the oil and the acoustic velocity in the oil. If the properties of the oil are unknown, the thickness estimate would be accurate to about $\pm$20%.

For either a low-power laser or a radar source the individual pulse response will be below background noise levels; however, the average power resulting from modulated cw irradiation can result in a relatively powerful acoustic signal. The pulse repetition frequency (PRF) could be swept through the film resonance frequency (Fiorito and Uberall 1979; Fiorito et al. 1986). However, calculations indicate that, depending on assumptions on the location of the source, acoustic energy in the film will increase only a few dB at exact resonance because of the close match in acoustic impedance between oil and water. Therefore, detection of resonant peaks as a function of frequency will not be successful, and single high-power pulses should be used.

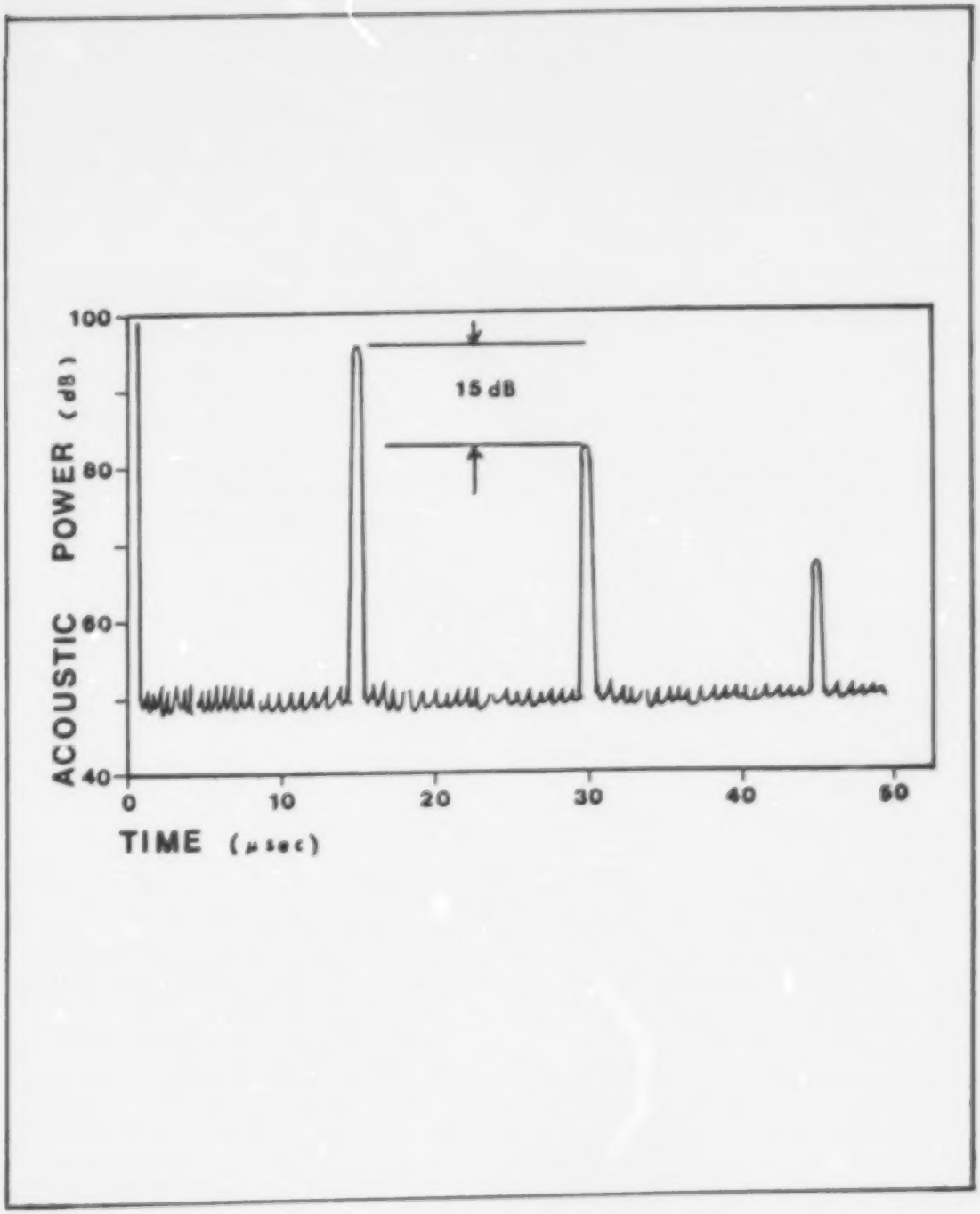

Figure 19 Idealized acoustic response from an oil layer about 20 mm thick stimulated by a short, high-power laser pulse. The noise floor shown is typical of ambient noise in the ocean at frequencies around 1 MHz (50 dB re: 1 uPa).

2.4 DETECTION OF THERMOELASTIC RESPONSE

2.4.1 Acoustic methods

Acoustic detection methods could be considered for the remote detection of the thermoelastic response. Ideally an acoustic receiver would be mounted on the aircraft. Alternately a hydrophone might be deployed from the aircraft for monitoring acoustic response from the water below the oil slick.

The attenuation of sound in air (neglecting spreading losses) can be approximated by:

$$A = 8.686\ (1.83 \times 10^{-11}\ f^2) \qquad [2.9]$$

where A is attenuation in dB/m and f is frequency in Hz (Mason and Thurston 1984).

The frequency range of interest is from 500 KHz to 10 MHz (see Figure 18). The corresponding attenuation rates are 40 dB/m to 16,000 dB/m. These attenuation values suggest that, even for lower frequencies around 1 MHz, the maximum reception range through air would be less than one metre, and therefore this detection technique would not be suitable.

For a hydrophone located in the water under a slick the situation is somewhat better. Attenuation rates range from 0.2 dB/m at 1 MHz to 20 dB/m at 10 MHz, as shown in Figure 20 (Urick 1983). Ambient noise in the ocean at these frequencies is primarily thermal noise. Noise intensities calculated from the Boltzmann equation, as shown in Figure 21 (Mitson 1983), indicate background noise levels in the order of 50 dB re: 1 uPa.

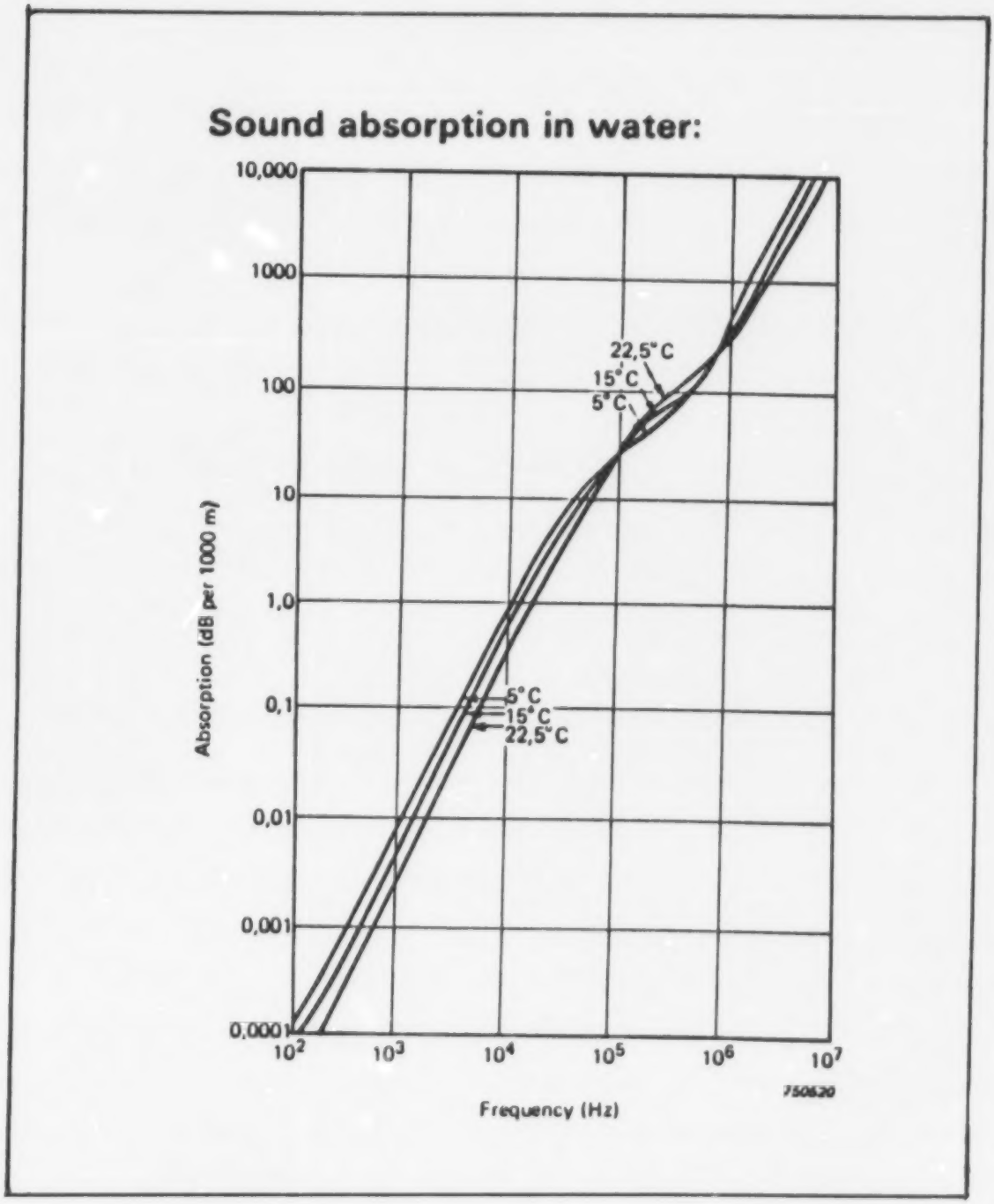

Figure 20 Attenuation rates of sound in water as a function of frequency (after Bruel and Kjaer application notes)

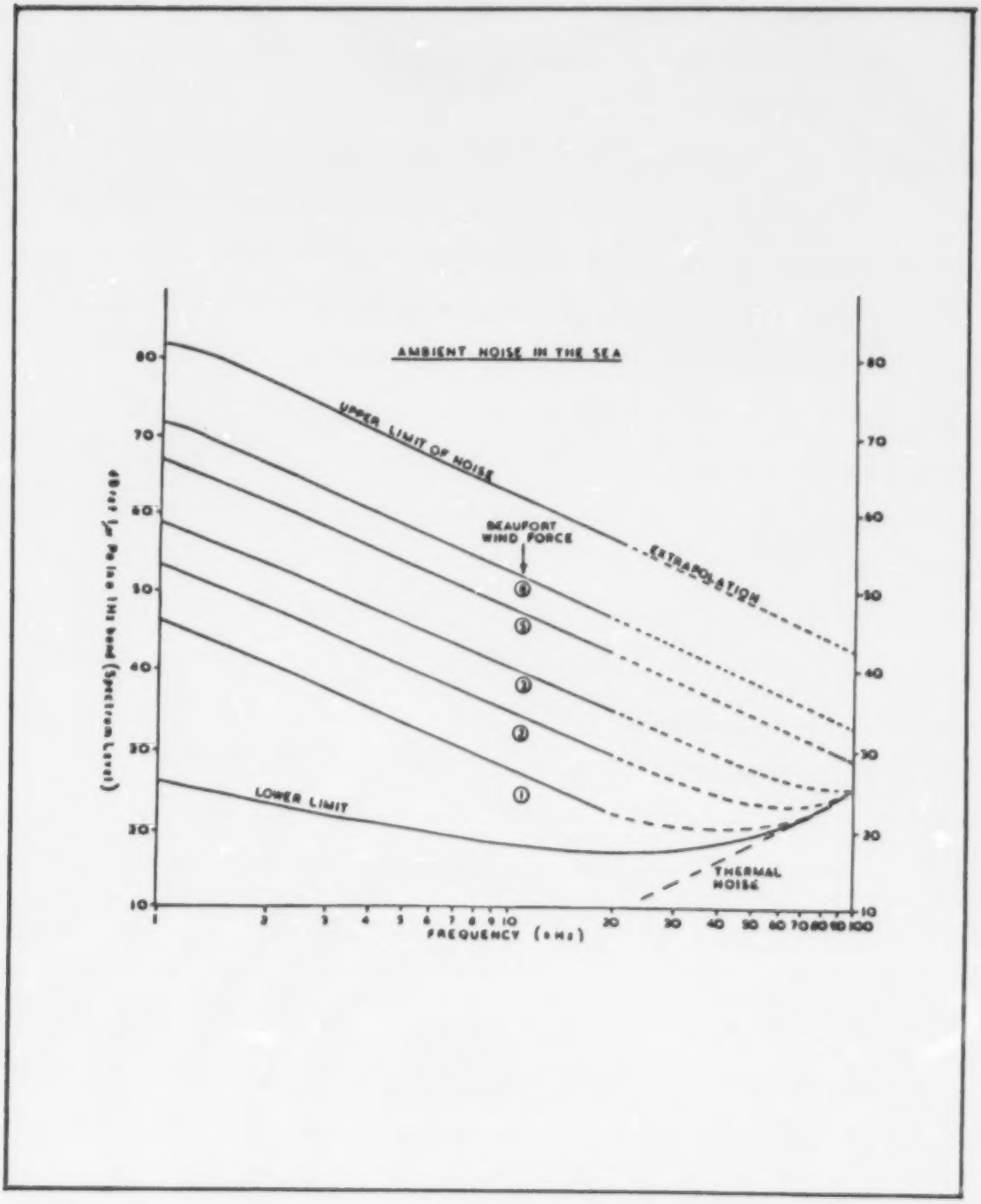

Figure 21 Ambient acoustic noise in the ocean as a function of frequency. By extrapolation, at frequencies above 1 MHz thermal noise will dominate, and can be calculated using the Boltzmann equation (after Mitson 1983).

Calculations in Section 2.2 indicated that acoustic signal levels in the order of 116 dB could be generated. If 6 dB is set as the minimum signal-to-noise ratio for detection by hydrophone then losses in the order of

$$116 - (6 + 50) = 60 \text{ dB} \qquad [2.10]$$

can be tolerated. At approximately 1 MHz, with $A = 0.5$ dB/m, this method would allow a detection range of 120 m. However, at the upper end of the spectrum, at 10 MHz, A is greater than 10 dB/m and the detection range would be limited to a few metres. Therefore, a hydrophone detector would have a working range of a few metres for thin slicks, and several tens of metres for thicker oil layers.

2.4.2 Optical Interferometry

Optical interferometry is extensively used for precision metrology and is an alternative to acoustic detection of thermoelastic displacement. The normal working range for interferometers is less than 1 metre with resolution of a few nanometres. However, working ranges as large as 60 m have been achieved and displacements as small as 0.1 pm can be detected (Monchalin 1985a; 1985b). Theoretical detection limits are in the order of 10^{-16} m for visible light interferometry (Monchalin 1986). For industrial applications in which immunity to vibration, air turbulence, and insensitivity to alignment are important, a Fabry-Perot type of velocity interferometer is recommended.

Monchalin has developed two different interferometer systems for optical detection of laser generated ultrasonic pulses.

Heterodyne laser interferometry and Fabry-Perot velocity interferometry have been applied successfully to problems of detection of remote optical vibration in noisy industrial environments.

Brown and Wyeth (1983) have reported the use of an interferometric technique for detection and measurement of a microwave-induced thermoelastic response in eye lenses. The system detects motions in the order of a few nm as a result of irradiation at about 920 MHz with pulse duration of 10 us and intensity of about 1 MW/m2.

As shown in Section 2.2, the displacements expected for electromagnetic thermoelastic emission are in the order of 10 nm to 0.1 pm. Optical interferometry systems are sensitive enough to detect these displacements, and a laboratory confirmation is described in Chapter 3.

2.5 SUMMARY

Several types of portable electromagnetic energy sources could deliver peak irradiation intensities in the order of 10^4 to 10^{10} W/m^2 at 20 m range. The calculated thermoelastic response for each of these sources indicated that average acoustic energy intensities of 86 to 116 dB re: 1 uPa could be achieved for oil layers on water. The calculated mechanical displacement associated with the thermoelastic pulse are in the order of 10 nm for a high-power Nd:Yag laser pulse and in the order of 0.1 pm for a 100-W, modulated, CO_2 laser or a 25 kW X-band radar. Although the resulting average acoustic signal strength is well above background noise levels, attenuation in air precludes use of an

air-coupled microphone as a detector. Hydrophones in the water might detect the signal, but estimation of layer thickness by resonance frequency of the oil layer is not promising.

Optical interferometry methods can detect displacements as small as 10^{-16} m at working ranges of several metres. This sensitivity is more than adequate for detection of thermoelastic displacements generated by a pulse laser.

The conclusion is that a practical slick thickness measurement system could be based on:

- a high-energy pulsed laser as an irradiation source;
- detection of single pulse echo reverberation in the oil film; and
- optical interferometer for detection of displacement associated with the thermoelastic pulse.

3. EXPERIMENTAL VERIFICATION

Through the courtesy of Dr. J.P. Monchalin and his colleagues at the Industrial Materials Research Institute (IMRI) of the National Research Council of Canada in Montreal, we were able to verify experimentally the feasibility of the slick thickness measurement system outlined in Section 2.5. The laboratory experiment demonstrated velocity interferometry for optical detection of thermoelastic pulse reverberation in a layer of oil on water.

3.1 METHOD

The system that was used is depicted in Figure 22. It consisted of a J and K Nd:Yag excitation laser capable of delivering a 10-ns pulse at about 1-um wavelength with energy up to 1 J. This energy was focused to a spot size of a few millimetres in diameter on a 1-cm layer of Hibernia crude oil in a beaker of tap water.

A velocity interferometer using a 1-W J and K Argon laser and a 50-cm Fabry-Perot interferometer was used to detect the elastic pulse and the subsequent reverberations at a working range of about 1 m. A schematic sketch of the interferometer is also shown in Figure 22.

Detected amplitudes of the elastic reverberations were recorded both with the beaker stationary and oscillating.

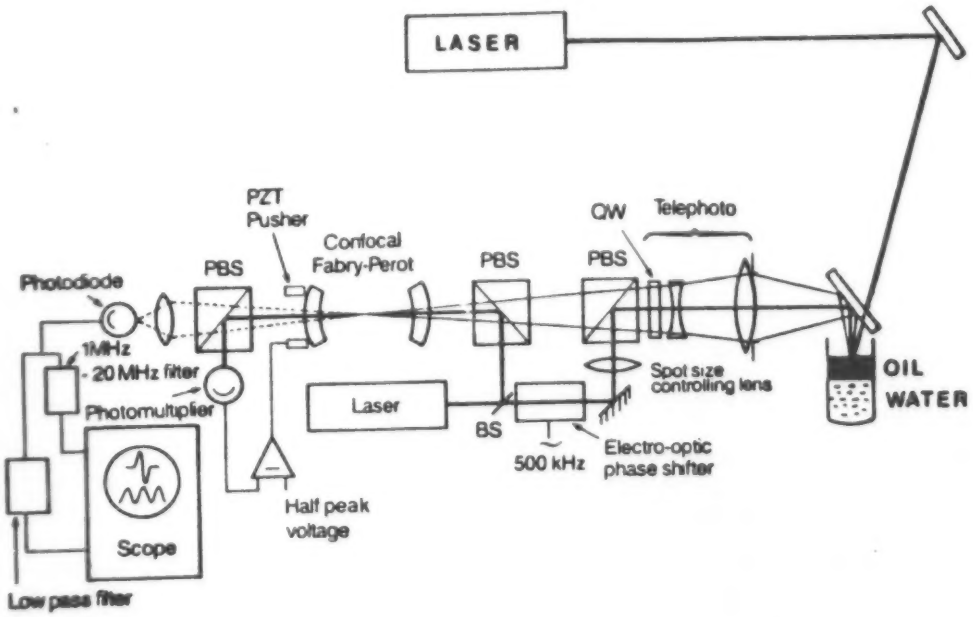

The upper source laser is pulsed Yag focused on the oil surface. The lower equipment shows the interferometer for detection of the response: (BS) beamsplitter; (BPS) polarizing beamsplitters (reflect nearly 100% of the light polarized perpendicularly to the plane of the drawing and transmit nearly 100% of the light polarized in the plane of the drawing); (QW) quarter-wave plate oriented at 45^{o} to the laser polarization. A lens is used to produce the proper spot size on the sample through the telephoto lens.

Figure 22 Experimental set-up for testing interferometric detection of oil film thermoelastic response (diagram adapted from Monchalin 1986)

3.2 RESULTS

A set of measurement results is seen in Figure 23. The initial pulse is followed by a reflection from the oil-water interface at about 20-us delay corresponding to an oil layer about 1.3 cm thick, assuming acoustic velocity of 1,300 m/s. Reflections from the sides of the beaker (in the oil film) follow at 23 to 35 us, and reflections from the bottom of the beaker are at 55 to 60 us.

The measurement capacity of the experimental system was quite insensitive to motion and low frequency vibration in the sample.

Specular reflection from the oil surface provided a strong interferometer signal. The excitation laser was not well matched to the oil properties. It was shown in Section 2.2 that for Yag illumination at about 1 um wavelength and a pulse length of about 10 ns, CT is 10^{-2}, and the thermoelastic conversion efficiency is about two orders of magnitude smaller than for an optimum system. For example, a CO_2 laser source operating at 10 um with an equivalent pulse energy could be more effective.

The working range of this system was about 1 m with a depth of focus of about 100 mm. Dr. Monchalin did not see any difficulty in extending the working range to 20 m by increasing the aperture of the telephoto lens. The interferometer sensitivity could also be substantially increased by using a higher power interferometer laser. A 1-kW, long pulse, low-noise laser is currently being assembled at IMRI for this purpose.

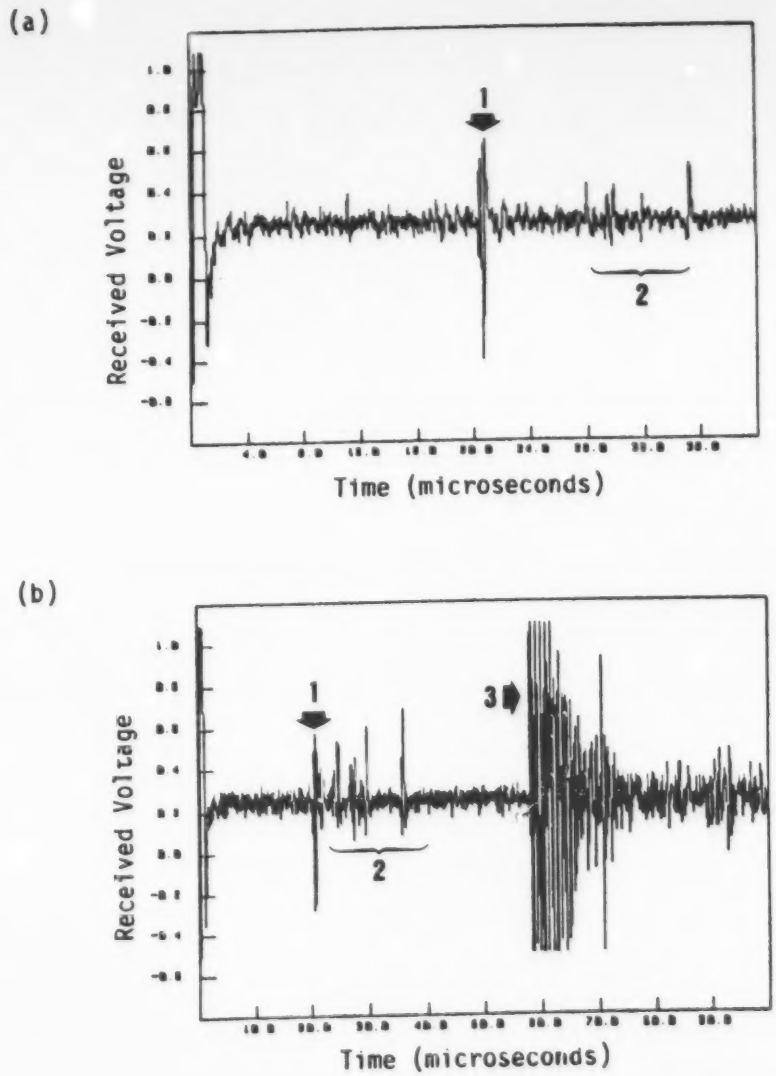

The Yag laser pulse occurs at time zero. The first reflection from the oil water interface is seen after a 20 us delay (1). Subsequent echoes arrive from the sides of the beaker (2) and from the bottom of the beaker (3).

Figure 23 Experimental test results with two different time scales

3.3 CONCLUSIONS

The results presented, although for a relatively simple laboratory example, verify dramatically the order of magnitude theory given in Chapter 2; i.e.,

- laser excitation of oil on water is able to induce thermoelastic emission;
- conversion efficiencies, although small, provide a detectable elastic response;
- optical interferometry is able to detect the elastic response;
- the resulting signal provides a measurement of oil thickness;
- the measurement is not sensitive to low-frequency vibration in the oil/water.

The thickness accuracy in the measurement will be limited primarily by the lack of knowledge of acoustic speed in the oil. Given the variability in properties of oils, this uncertainty might be as much as $\pm$20%.

4. SYSTEM DESIGN AND RECOMMENDATIONS

A preliminary airborne system design is outlined here in order to identify the necessary system functions and the components required to meet reasonable performance criteria. A suggested operating scenario, shown in Figure 24, indicates a system operated from a helicopter or other small aircraft flying at an altitude of 20 m and at a speed less than about 50 m/s (100 knots). The system should be capable of sampling the ocean surface intermittently with a footprint diameter of a few centimetres. Equipment should be portable and installable in a variety of aircraft without major modifications to the equipment or to the aircraft. The system should be capable of measuring slick thicknesses from 0.1 mm to 10 mm.

4.1 SYSTEM DESCRIPTION

A system block diagram is shown in Figure 25 and is described briefly here.

4.1.1 Optical unit

A high-energy laser (4), operating in the infra-red at 0.1 to 1.0 J/pulse and with a PRF of at least 100 Hz, is the illumination source. This laser would be focused to a footprint diameter of about 20 mm by a telescope (7) with automatic surface tracking focus supplied by an optical rangefinder (9) and driver (3), and motor (6). The thermoelastic displacement and the reverberation of the acoustic wave would be detected (11) through an interferometer (10) with range resolution of 0.1 nm. The inter-

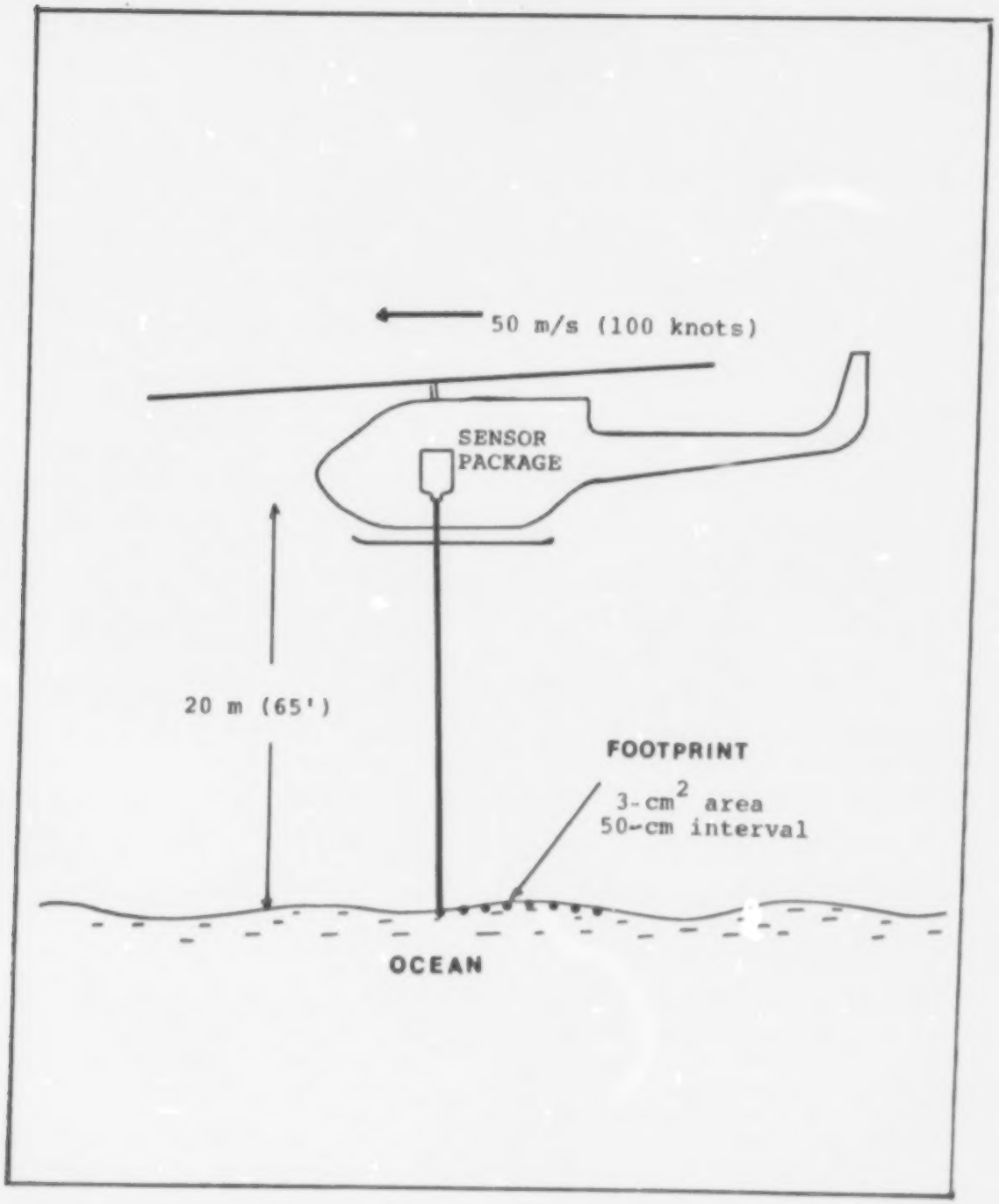

Figure 24 Operating scenario for oil slick thickness measurement system. Helicopter mounted, maximum altitude about 20 m, maximum speed about 50 m/s, footprint size about 2 cm diameter, footprint spacing about 0.5 m.

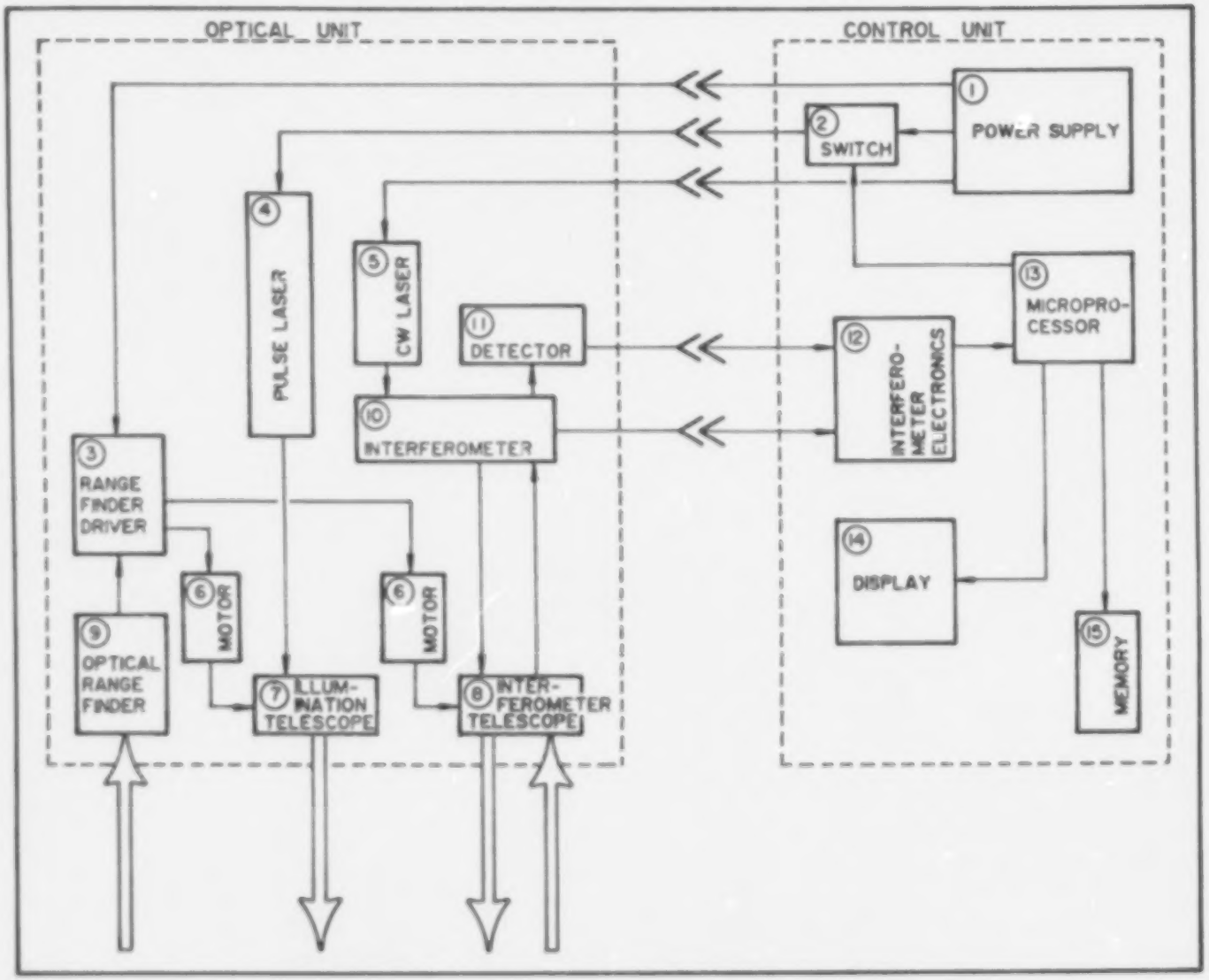

Figure 25 Oil slick thickness measurement system block diagram

ferometer would include a cw laser source (5) and a surface tracking telescope (8) driven by the rangefinder (3) and motor (6).

4.1.2 Control unit

The interferometer electronics package (12) would feed displacement information to a microprocessor (13) for interpretation. The microprocessor unit would display (14) and store (15) oil thickness information in a suitable format. The microprocessor would also control the firing of the pulse laser (4) via a switch (2) so that the pulse is initiated at times when high specular reflection provides best sensitivity at the interferometer (10). Power is distributed to all components from supply (1).

4.1.3 Discussion

A typical system timing sequence is outlined in Table 8. For a slick 0.1 mm thick the pulse echo reverberation time is in the order of 1.5×10^{-7} seconds. Therefore to detect five reverberation cycles, the detection interval must be about 1 us. For a slick of 10-mm thickness, it must be about 100 us. During this time the sensor will move about one-quarter of the footprint. The PRF will need to be greater than 100 Hz to achieve a 0.5-m sampling interval over the ocean.

The operating wavelength and pulse duration of the illumination laser must be selected with reference to the minimum slick thickness to be measured and to the attenuation coefficient of oil at the laser wavelength. As discussed in Section 2.1, electromagnetic to acoustic conversion efficiency is greatest when the pulse

Table 8

Oil slick thickness measurement system timing sequence

1.	Power up all active devices and prime laser.
2.	If detector indicates sufficient backscatter for measurement, fire laser within 1 us (target motion @ 100 knots = 50×10^{-6} m).
3.	Detect thermoelastic pulse reverberation for 100 us (target motion @ 100 knots = 5 mm, about 1/4 footprint diameter).
4.	Display and store oil layer thickness measurement.
5.	Repeat measurement at 10 ms interval or when backscatter is sufficient (sampling interval @ 100 knots = 0.5 m).

length is matched to the attenuation distance in the oil, which implies that relatively high absorption in the oil is optimum. From Table 4, this condition is best satisfied at a wavelength of about 10 um. Suitable CO_2 lasers are available in portable packages.

The interferometer and its associated sub-systems are non--standard devices which would have to be custom designed for this application; their functional requirements are close to state-of-the-art. Design trade-offs will occur between the coherence length and power of the interferometry laser and the aperture and depth of the focus of the interferometry telescope. A large aperture relaxes the laser power requirements but places higher demands on the surface tracking capability of the telescope, range finder, and driver.

Other trade-offs will occur between the power of the il-

lumination laser and the measurement laser. The interferometer's resolution requirements might be relaxed slightly by increasing the power of the illumination laser; the interferometer's sensitivity could be increased by increasing the power of the measurement laser.

The electronic components in the control unit as well as the illumination laser telescope and rangefinder could be assembled using off-the-shelf equipment.

The design, development and testing of a suitable airborne package would cost between $250,000 and $1,000,000. After development systems might be reproduced at a cost of about $100,000 to $200,000 per unit.

4.2 RECOMMENDATIONS

The technique of thermoelastic excitation and interferometric detection for remote oil slick thickness measurement appears feasible. A laboratory test confirmed theoretical predictions. A preliminary system design suggests that performance requirements could be met with current capability.

However, development costs of an airborne system will probably be substantial. Therefore, it is recommended that a more thorough experimental evaluation be made. A more optimum illumination laser should be used than in the experiment described in Chapter 3. Prototype interferometry equipment could likely be obtained from the Industrial Materials Research Institute in Montreal.

The experiment could be made in a controlled test tank with wave-generating apparatus. The sensor equipment could be mounted a few tens of metres above the tank. The objectives of the experiment

would be to refine limits of operating performance, particularly for rough oceans conditions, and to examine the design trade-offs and costs of an operating system. In a controlled environment, known amounts of oil could be introduced into the tank. Experiments could be run with various wave conditions, oil thicknesses, and detector ranges.

This set of experiments might be conducted in conjunction with similar experiments recommended for the oil slick thickness measurement technique described in Part A of this report, active microwave spectroscopy. In this way maximum use would be made of the tank since many of the operating conditions would be similar for the two sets of experiments.

APPENDIX A
PHYSICAL DISPLACEMENT CALCULATION

The physical displacement associated with the energy absorbed can be derived approximately from Love's stress-strain relationship (Gournay 1966) for a heated medium as follows:

$$\varepsilon = \frac{\sigma}{B} + \beta\,\theta \qquad [A.1]$$

where ε is the strain
σ is the stress
B is the elastic modulus = C2 .

$$\theta = \frac{\alpha I_o T e^{-\alpha x}}{\rho QS} \qquad [A.2]$$

where α = attenuation coefficient and x is the depth.
Other parameters are as defined in Table 2.

$$\sigma = \frac{C \beta I_o}{2QS}(1-e^{-\alpha CT/2}) \qquad [A.3]$$

which approaches a limiting value of

$$\sigma = \frac{C \beta I_o}{2QS} \quad \text{for } \alpha CT >> 1 \qquad [A.4]$$

for either a free or constrained surface.
Combining equations A.1 - A.4,

$$\varepsilon = \frac{\beta I_o}{\rho QS}\left(\frac{1}{2C} + \alpha T e^{-\alpha x}\right) \qquad [A.5]$$

Setting $x = \frac{1}{\alpha}$ and $T = \frac{1}{\alpha C}$ (both are reasonable conditions for the problem at hand):

$$\varepsilon \simeq \frac{\alpha \beta I_o T}{\rho QS} \qquad [A.6]$$

The displacement Δx in metres can be estimated from

$$\Delta X \simeq x\,\varepsilon = \frac{\beta I_o T}{\rho QS} . \qquad [A.7]$$

REFERENCES

Beckmann, P. and A. Spizzichino. 1963. The scattering of electromagnetic waves from rough surfaces, Macmillan, New York, N.Y. 503 p.

Blitz, J. 1967. Fundamentals of ultrasonics. Second Edition. Plenum Press, New York, N.Y.

Borth, D.E. and C.A. Cain. 1977. Theoretical analysis of acoustic signal generation in materials irradiated with microwave energy. IEEE Transactions on Microwave Theory and Techniques MTT-25 (11): 944-954.

Brekhovskikh, L.M. 1960. Waves in layered media, Academic Press, New York, N.Y. 561 p.

Brown, P.V.K. and N.C. Wyeth. 1983 Laser interferometer for measuring microwave induced motion in eye lenses in vitro. Review of Scientific Instruments. 54 (1): 85-89.

Butt, K.A. and J. B. Gamberg. 1980. Technology of an airborne impulse radar. Proceedings of the international workshop on the remote estimation of sea ice thickness, St. John's, September 25-26, 1979, C-CORE Technical Report 80-5: 385-412.

C-CORE. 1978. Investigation of the use of microwave systems in detection and monitoring oil slicks over ice and ice- infested waters. C-CORE Technical Report 78-18: 196-215.

DuHamel, R.H. amd G.G. Chadwick. 1984. Frequency-independent antennas. p. 14-1 to 14-43 In: R. C. Johnson and H. Jasik (editors), Antenna Engineering Handbook, McGraw-Hill, New York. N.Y. p. 14-1 - 14-43.

Fiorito, R., W. Madigosky and H. Uberall. 1986 . An exact resonance decomposition of acoustic transmission and reflection coefficients of a fluid layer. Journal of Acoustical Society of America 79 (2): 222-231.

Fiorito, R. and H. Uberall. 1979. Resonance theory of acoustic reflection and transmission through a fluid layer. Journal of Acoustical Society of America 60 (1): 9-14.

Gournay, L.S. 1966. Conversion of electromagnetic to acoustic energy by surface heating. Journal Acoustical Society of America. 40 (6): 1322-1330.

Iizuka K. and A.P. Freundorfer. 1983. Detection of nonmetallic buried objects by a step frequency radar. Proceedings of the IEEE, 71 (2): 276-279.

Jones, H.W. amd H.W. Kwan. 1983. The detection of crude oil under seawater in the arctic ocean. Proceedings of the Sixth Arctic Marine Oilspill Program Technical Seminar, Edmonton: Environmental Protection Service, Ottawa, Ontario: 241-252.

Jones, H.W. and E. Yeatman. 1985. The visco-elastic properties of 'weathered' crude oil from the Beaufort Sea. Journal of Acoustical Society America 78 (2): 801-802.

Lin, J.C. 1977. Further studies on the microwave auditory effect. IEEE Transactions on Microwave Theory and Techniques MTT-25 (11): 938-943.

Lin, J.C. and K. Chan. 1984. Microwave thermoelastic tissue imaging - system design. IEEE Transactions on Microwave Theory and Techniques MTT-32 (8): 854-860.

MacDougall, J.W. and J.K.E. Tunaley. 1986. The complex permittivity of crude oil. Proceedings of the Ninth Arctic Marine Oilspill Program Technical Seminar, Edmonton. Environmental Protection Service, Ottawa, Ontario: 413-420.

Mason, W.P. and R.N. Thurston. 1984. Physical acoustics principles and methods. XVII, Academic Press, Inc. 326 p.

Mazda, F. 1984. Electronic engineers reference book. Butterworth's, Toronto, Ontario.

Mitson, R.B. 1983. Fisheries sonar. Fishing News Books, Surrey.

Monchalin, J.-P. 1986. Optical detection of ultrasound. IEEE Transactions on Ultrasonics, Ferroelectrics and Frequency Control UFFC-33 (5): 485-499.

Monchalin, J.-P. 1985a. Heterodyne interferometric laser probe to measure continuous ultrasonic displacements. Review of Scientific Instruments 56 (4): 543-546.

Monchalin, J.-P. 1985b. Optical detection of ultrasound at a distance using a confocal Fabry-Perot interferometer. Applied Physics Letters 47 (1): 14-16.

Morey, R.M. 1974. Continuous subsurface profiling by impulse radar. Proceedings of Engineering Foundation Conference on 'Subsurface Exploration for Underground Excavation and Heavy Construction', American Society of Civil Engineers, New York, N.Y. 213-232.

Rossiter, J.R., P. Langhorne, T. Ridings and A.J. Allan. 1977. Study of sea ice using impulse radar. Proceedings of the Fourth International Conference on Port and Ocean Engineering under Arctic Conditions, St. John's, Sept. 26 - 30, 1977. 556-567.

Royer, G.M. 1973. The dielectric properties of ice, snow and water at microwave frequencies and the measurement of the thicknesses of ice and snow layers with radar. Communications Research Centre, Ottawa, Ontario. Report 1242: 32 p.

Scruby, C.B. 1986. Studies of laser-generated ultrasonic waveforms at different orientations. Applied Physics Letters 48 (2): 100-102.

Sears, F.W. 1949. Optics. Addison-Wesley Publishing Company, Reading, Mass. 386 p.

Sorensen, B. 1984. Danish airborne oil pollution monitoring and coastal surveillance system: state of the art and beyond. Remote sensing for the control of marine pollution. Plenum Press, New York, N.Y. p. 71-86.

Urick, R.J. 1983. Principles of underwater sound. Third Edition, McGraw-Hill Book Company, New York, N.Y. 423 p.

Vant, M.R. 1976. A combined empirical and theoretical study of the dielectric properties of sea ice over the frequency range 100 MHz to 40 GHz. Ph.D. Thesis, Carleton University, Ottawa, Ontario. 438 p.

Von Hippel, A.R. 1954. Dielectric materials and applications. Massachusetts Institute of Technology, Cambridge, Mass. 438 p.

Weaver, H.J. 1983. Applications of discrete and continuous fourier analysis. John Wiley & Sons, New York, N.Y.

West, G.A., J.J. Barrett, D.R. Siebert and K.V. Reddy. 1983. Photoacoustic spectroscopy. Review of Scientific Instrumemts. 54 (7): 797-817.

White, R.M. 1963. Generation of elastic waves by transient surface heating. Journal of Applied Physics 34 (12): 3559-3571.